The Role of Convective-Scale Precipitation Downdrafts in Cumulus and Synoptic-Scale Interactions

RICHARD H. JOHNSON[1]

National Hurricane and Experimental Meteorology Laboratory, NOAA, Coral Gables, Fla. 33124

(Manuscript received 9 February 1976, in revised form 16 June 1976)

ABSTRACT

A diagnostic model has been developed to determine the contribution by convective-scale precipitation downdrafts to the total cumulus fluxes of mass, heat and moisture on the synoptic scale. Populations of cumulus clouds are assumed to consist of individual cloud elements of various sizes, each possessing an updraft and downdraft that are modeled as steady-state, entraining plumes. An integral equation for a function representing the cloud base mass flux for each type of cloud is derived based on an assumption regarding the relative intensities of the updraft and downdraft.

The model is tested on the Reed and Recker (1971) western Pacific composite easterly wave data and on a heavy-rain-producing tropical depression that occurred over northern Florida in 1969. Results from both studies indicate that cumulus downdrafts contribute significantly to the total convective mass transport in the lower troposphere. It is shown that the neglect of cumulus downdrafts and their associated rainfall evaporation leads to the diagnosis of excessively large populations of shallow cumulus clouds in highly convective situations. Analysis of the subcloud-layer moisture budget shows downdraft water vapor transport to be important in the water vapor balance for this layer. The implications of the findings of this diagnostic study on theories for the parameterization of cumulus convection are discussed.

1. Introduction

A number of recent research efforts, including the 1974 GARP Atlantic Tropical Experiment (GATE), have sought, through various approaches, to clarify the nature of the interaction between small-scale cumulus convection and the large-scale circulation of the troposphere. Much attention is currently being given to the diagnostic study of the interaction processes. Yanai *et al.* (1973) have developed a diagnostic method for the determination of the bulk or averaged properties of populations of cumulus clouds from observations of large-scale meteorological variables. Methods have been developed by Ogura and Cho (1973) and Nitta (1975) which have enabled the spectral distribution of cumulus mass flux for populations of cumulus clouds to be diagnosed from large-scale variables. In studies of this nature the cumulus cloud has been modeled as a one-dimensional, steady-state entraining plume updraft. Precipitation formed within the updraft has been assumed to fall out instantaneously with no evaporation taking place. It has become increasingly evident, however, that in regions of active convection it may be necessary to take into account the effects of precipitation evaporation if a correct diagnosis of the properties of cumulus populations is to be made. This precipitation evaporation is responsible for maintaining negatively buoyant downdrafts which are present during the life cycle of individual cumulus clouds. In this paper a method is developed to estimate the contribution to the total convective mass, heat and moisture transports by cumulus-scale precipitation downdrafts.

Observations of cumulus clouds of all sizes have revealed convective-scale downdrafts to be important features of cloud circulations. The first extensive quantitative measurements of such downdrafts within cumulonimbus clouds were made during the Thunderstorm Project (Byers and Braham, 1949). Based on data gathered from nearly 1400 aircraft flights into cumulonimbi over Ohio and Florida, the downdraft was identified as a prominent feature in the thunderstorm life cycle. It was found that, in general, the most intense draft velocities occurred during the mature stage of thunderstorm development and that, except near cloud top, downdraft velocities and widths averaged only 15–20% less than those of the adjacent updraft (Braham, 1952). Braham computed average thunderstorm-cell vertical mass fluxes from aircraft measurements made during the project, finding that the downdraft mass flux increases from 400 to 900 mb, reaching at cloud base a magnitude equal to one-half the peak updraft mass flux that occurs at the 500 mb level. Further, with regard to the important role in the cloud water budget, he determined that over 45% of

[1] The bulk of this work was completed at the University of Washington, Seattle.

the total condensed water in the average storm was later reevaporated in precipitation downdrafts.

Riehl and Malkus (1958) proposed that cumulonimbus downdrafts play an important role in the total energy transport in tropical regions. In an analysis of the heat budget in the equatorial trough region, they determined that saturated cumulonimbus downdrafts accompanying updrafts must be taken into account if a proper heat balance is to be achieved. A more detailed examination of cumulus-scale downdrafts in tropical convective systems was made by Riehl and Pearce (1968) in the western Caribbean. By analyzing the equivalent potential temperature (θ_e) structure of the troposphere before and after the passage of several tropical wave disturbances, the authors concluded that prolonged downdraft activity must have occurred to produce the consistently observed reduction in θ_e in the lower troposphere on the synoptic scale following passage of disturbances.

A similar conclusion can be drawn from the Reed and Recker (1971) composite of 18 westward propagating tropical wave disturbances that passed through the western Pacific islands of Kwajalein, Eniwetok and Ponape in the summer of 1967. A vertical cross section of moist static energy and deviations from the mean has been constructed for their composite wave (Fig. 1). Moist static energy, defined by $h \equiv c_pT + Lq + gz$, where T is temperature, z geopotential height, q specific humidity, c_p specific heat of air at constant pressure, g acceleration of gravity and L latent heat of condensation is approximately conserved, as is θ_e under moist adiabatic motion. Of particular interest are the positive anomaly in the mid-troposphere and the negative anomaly below 900 mb at and immediately to the rear of the axis of the wave trough. Both cooling and drying are found to contribute to the negative anomaly. The air flow relative to the trough is from west to east which puts this minimum just downstream from the position of heaviest observed precipitation. Reed and Recker suggest that modulation of radiative heating by cloud cover is probably not an important factor in producing the cooling observed in this region (see their Fig. 5) because this feature is also present at night. This leaves as the only feasible explanation for the negative anomaly the transport of relatively cool and originally dry mid-tropospheric air (Fig. 1, top) into the subcloud layer by active downdrafts.

Another confirmation of the substantial contribution to total convective transport by cumulus downdrafts in equatorial regions was provided by Betts (1973a) in a study of Venezuelan thunderstorms. Mass fluxes in cumulus downdrafts determined from the compositing of rawinsonde observations taken in the region of deep convective cells during their growing and decaying stages were found to be about one-half the size of those in cumulus updrafts through the depth of the troposphere below 400 mb.

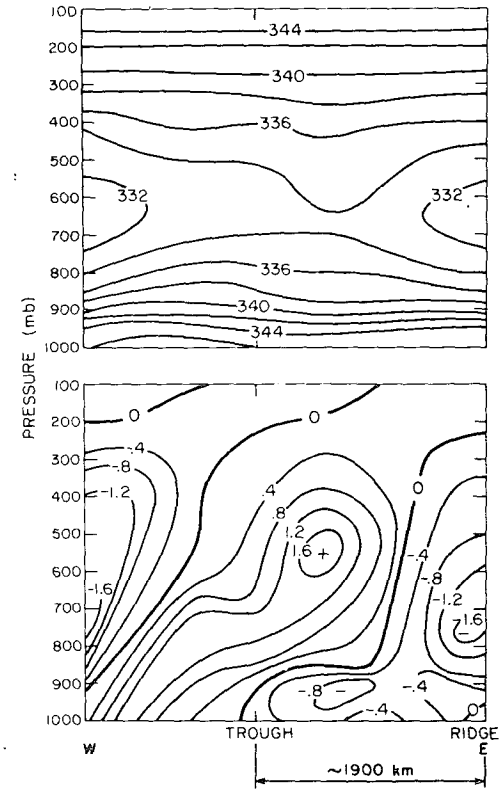

FIG. 1. Moist static energy for Reed and Recker composite wave (top) and deviations from mean (bottom). Units: J g^{-1}.

It is commonly assumed that cumulus convection, having a length scale ~1–10 km, somehow responds directly to forcing by the large-scale flow (length scale ~10^3 km). There is ample evidence to indicate that this is the case for many convective tropical systems. The possibility exists, however, that under some circumstances one or more intermediate scales may have a crucially important effect on the response of the cumulus convection or may even independently determine the nature and character of the convective activity. This possibility has been discussed by Zipser (1970), Betts (1974) and others. Measurements by Zipser (1969) and the numerical modeling results of Brown (1974) indicate that mesoscale downdrafts (length scale ~10^2 km) may contribute importantly to the total convective mass flux on the synoptic scale. In this paper any contribution to the large-scale mass transport that might occur due to mesoscale downdrafts is neglected at the outset as the effort is made to isolate the effects of convective-scale downdrafts.

One would expect the penetration of cumulus downdrafts into the layer below cloud base to have a pronounced influence on the heat and moisture stratification within this layer, as well as on the sensible and latent heat transfer from the ocean (or land) surface. Garstang (1967) has demonstrated, using data gathered over the tropical Atlantic Ocean, that marked en-

hancement of the latent and sensible heat transfer from the sea surface occurs when synoptic-scale disturbances are present. Convective downdrafts, by bringing relatively cool air down to the surface, could contribute substantially to the enhanced exchanges.

Betts (1973b) and Arakawa and Schubert (1974) have developed models for the subcloud layer that take into account the effect of cumulus updraft mass transports. The study of Esbensen (1975) indicates that accurate modeling of the mixed layer in large-scale prediction models requires separate specification of cumulus and small-scale eddy fluxes at the mixed-layer top. Ogura and Cho (1974) adopted this approach in their analysis of subcloud layer and cloud layer interaction for the convectively disturbed regions of Reed and Recker's (1971) composite tropical wave. A very interesting result of their study is that the detrainment from the subcloud layer of water vapor into ascending cumulus clouds and the entrainment from the compensating between-cloud subsidence contribute effects which are nearly an order of magnitude larger than any others in the moisture budget for this layer. Here again, however, the effects of cumulus-scale downdrafts have been neglected. The substantial downward transport of water vapor into the subcloud layer by active downdrafts has important consequences on the moisture budget for this layer as will be shown in the course of this paper. In addition, the model that is developed will permit estimates to be made of the contribution to the moisture budget by rainfall evaporation.

2. Theoretical development

a. *Basic equations for large-scale thermodynamic variables*

Consistent with the procedures and notation of previous works (Yanai *et al.*, 1973; Ogura and Cho, 1973; Nitta, 1975; and others) we average the heat and moisture equations over an area large enough to contain a statistically representative population of cumulus clouds, yet small compared to the synoptic scale to obtain

$$Q_1 \equiv \frac{\partial \bar{s}}{\partial t} + \nabla \cdot \bar{s}\bar{\mathbf{v}} + \frac{\partial}{\partial p}\bar{s}\bar{\omega} = L(\bar{c}-\bar{e}) + Q_R - \frac{\partial}{\partial p}(\overline{s'\omega'}), \quad (1)$$

$$Q_2 \equiv -L\left(\frac{\partial \bar{q}}{\partial t} + \nabla \cdot \bar{q}\bar{\mathbf{v}} + \frac{\partial}{\partial p}\bar{q}\bar{\omega}\right) = L(\bar{c}-\bar{e}) + L\frac{\partial}{\partial p}(\overline{q'\omega'}), \quad (2)$$

where $s \equiv c_p T + gz$ is the dry static energy, $\mathbf{v}$ is the horizontal wind vector, ω the vertical p-velocity, q the water vapor mixing ratio, c the condensation rate, e the evaporation rate, Q_R the area-average net radiative heating rate, L the latent heat of condensation, p pressure and t time; the overbar designates a horizontal average and the prime, the deviation of a quantity from its horizontally-averaged value. Q_1 and Q_2 have been referred to by Yanai *et al.* (1973) as the apparent heat source and apparent moisture sink, since they provide a measure of the action of convective processes in heating and depleting moisture from the large-scale environment. These quantities can be determined from large-scale observations. It is assumed that the correlation terms involving $\mathbf{v}'$ and s', q' [omitted from (1) and (2)] are at least an order of magnitude less than those containing ω' correlated with s' and q'. Combining (1) and (2) we have

$$Q_1 - Q_2 - Q_R = -\frac{\partial}{\partial p}(\overline{h'\omega'}), \quad (3)$$

where $h \equiv s + Lq$ is the moist static energy.

b. *Model for the cumulus updraft and downdraft*

We begin by partitioning the large-scale mean mass flux $\bar{M}(\equiv\bar{\omega})$ into its basic components; M_u the mass flux in cumulus updrafts, M_d the mass flux in cumulus downdrafts and $\tilde{M}$ the environmental or between-cloud mass flux. All M's are defined positive upward. Thus

$$\bar{M} = M_u + M_d + \tilde{M}$$

and we further define M_c as the net cumulus mass flux

$$M_c \equiv M_u + M_d.$$

The approach taken here with regard to the modeling of the cumulus *updrafts* follows identically the steady-state, entraining plume model of Ogura and Cho (1973) and of Arakawa and Schubert (1974). They consider each cumulus updraft to have a characteristic entrainment rate λ which uniquely determines the cloud depth. Specifically, it is assumed that the fractional mass entrainment rate is constant for each cloud, i.e.,

$$\frac{1}{m_u(\lambda,z)}\frac{\partial}{\partial z}m_u(\lambda,z) = \lambda, \quad (4)$$

where $m_u(\lambda,z)d\lambda$ is the mass flux contribution from cloud updrafts (subscript u) with entrainment rates between $\lambda - d\lambda/2$ and $\lambda + d\lambda/2$. A continuum of cloud sizes or entrainment rates is assumed to exist which completely describes the cumulus population. Solving (4), we have

$$m_u(\lambda,z) = m_B(\lambda)\exp\{\lambda[z - z_B(\lambda)]\}, \quad (5)$$

where $m_B(\lambda)$ is the cloud base mass flux distribution function and $z_B(\lambda)$ is the height of the cloud base. The total upward mass flux at any level due to all cumulus updrafts which penetrate that level is

$$M_u(z) = \int_{\lambda=0}^{\lambda(z)} m_u(\lambda,z)d\lambda, \quad (6)$$

where $\lambda(z)$ is the entrainment rate for clouds having tops at the height z. Fig. 2 illustrates the fundamental features of this updraft model.

It is now proposed that cumulus downdrafts can be reasonably described by applying the one-dimensional entraining plume model used for the updrafts. There are insufficient measurements of downdraft structures at this time to confirm or reject this hypothesis. A serious question that must be considered in the modeling of the cumulus downdraft concerns the properties of the air that the downdraft is entraining. Malkus (1955) has made measurements within tropical tradewind cumuli which indicate that downdrafts incur substantial entrainment of air that has passed through the adjacent updraft. This situation may also frequently be the case for deep cumuli, especially when they exist in a wind-sheared environment. This effect, though possibly an important factor for both updrafts and downdrafts, has not been included in the model.

It is assumed that each updraft has an accompanying downdraft and both have the same fractional mass entrainment rate λ. If we then model downdrafts as inverted plumes, we have

$$\frac{1}{m_d(\lambda,z)}\frac{\partial}{\partial z}m_d(\lambda,z)=-\lambda, \tag{7}$$

where $m_d(\lambda,z)d\lambda$ is the mass flux contribution from cloud downdrafts (subscript d) with entrainment rates between $\lambda+d\lambda/2$ and $\lambda-d\lambda/2(m_d<0)$. For each cloud then

$$m_d(\lambda,z)=m_0(\lambda)\exp\{\lambda[z_0(\lambda)-z]\}, \tag{8}$$

where $m_0(\lambda)$ is the downdraft-originating-level mass flux distribution function and $z_0(\lambda)$ the downdraft originating level. This level, though not specified at this point, probably exists somewhere between mid-cloud and cloud top. As indicated, it is a function of the entrainment rate λ, i.e., of the cloud type. While we use the term "downdraft originating level" in this discussion, strictly speaking downdrafts originate somewhere above the level z_0. We assume that it is only when the downdraft reaches the level z_0 that it takes on a plume-like behavior with an increase in amplitude given by (8). It is assumed that the downward motion above z_0 contributes negligibly to the total convective mass flux. The total downward mass flux due to all cumulus downdrafts which pass through any level z is then

$$M_d(z)=\int_{\lambda=0}^{\lambda_0(z)} m_d(\lambda,z)d\lambda,$$

where $\lambda_0(z)$ is the entrainment rate for clouds whose downdraft originates at z. Since there is no contribution to $M_d(z)$ from the interval $\lambda_0(z)<\lambda<\lambda(z)$, then we can equivalently write the above as

$$M_d(z)=\int_0^{\lambda(z)} m_d(\lambda,z)d\lambda. \tag{9}$$

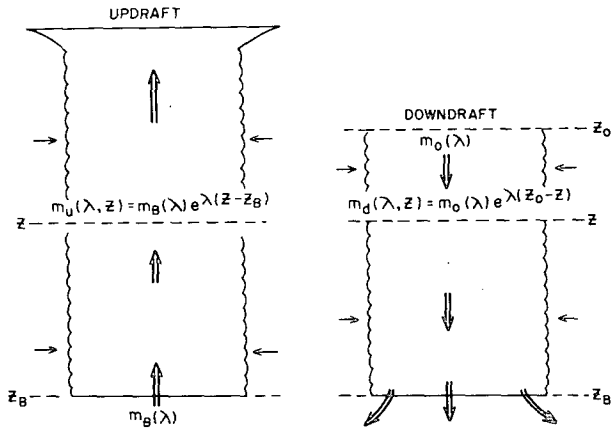

FIG. 2. Model for updraft and downdraft of cloud type λ. Units of $m_B(\lambda)$ and $m_0(\lambda)$ are mb km day^{-1}.

As Fig. 2 portrays, the updraft and downdraft are modeled as separate entities with interactions between the two being neglected; both entrain the same environmental air. Of course, it is understood that the downdraft is supplied with precipitation generated within the adjacent updraft so that a negatively buoyant downdraft may be maintained through precipitation drag and evaporation. Assumptions regarding detrainment from the clouds will be stated later. It is also noted here that updrafts and downdrafts need not have the same cross-sectional area; it is only assumed that every updraft has a corresponding downdraft. Obviously, this highly idealized model of the updraft and downdraft does not describe in detail all of the complex processes going on in convective regimes such as cumulonimbus line formation, cloud mergers, etc.; however, hopefully, it contains enough of the essence of these cumulus structures to provide an adequate basis for studying cumulus and synoptic-scale interactions.

The entrainment relations (4) and (7) are written with height z as the vertical coordinate. Transforming these equations into pressure coordinates we obtain for the updraft

$$\frac{1}{m_u(\lambda,p)}\frac{\partial}{\partial p}m_u(\lambda,p)=-\frac{\lambda H}{p}, \tag{10a}$$

and for the downdraft

$$\frac{1}{m_d(\lambda,p)}\frac{\partial}{\partial p}m_d(\lambda,p)=\frac{\lambda H}{p}, \tag{10b}$$

where $H\equiv R_dT_v/g$ is the scale height of an atmosphere with a virtual temperature $T_v\equiv T(1+0.608q)$ and R_d is the gas constant for dry air. The solutions of (10a, b) are then

$$m_u\equiv m_u(\lambda,p)=m_B(\lambda)\eta_u(\lambda,p), \tag{11a}$$

$$m_d\equiv m_d(\lambda,p)=m_0(\lambda)\eta_d(\lambda,p), \tag{11b}$$

where

$$\left.\begin{aligned}\eta_u(\lambda,p)&\equiv\exp\left(\int_p^{p_B(\lambda)}\frac{\lambda H}{p}dp\right)\\ \eta_d(\lambda,p)&\equiv\exp\left(\int_{p_0(\lambda)}^{p}\frac{\lambda H}{p}dp\right)\end{aligned}\right\},$$

$p_B(\lambda)$ is the cloud-base pressure level and $p_0(\lambda)$ the pressure level at which the downdraft originates.

Assuming that radiative heating plays only a minor role in the growth of individual cumulus clouds, the theory for a steady-state, entraining plume (Squires and Turner, 1962) leads to the following forms of the first law:

$$\frac{\partial}{\partial p}(m_u h_u)=\tilde{h}\frac{\partial m_u}{\partial p}, \tag{12a}$$

$$\frac{\partial}{\partial p}(m_d h_d)=\tilde{h}\frac{\partial m_d}{\partial p}, \tag{12b}$$

for the updraft and downdraft, respectively. As has been shown previously by Ogura and Cho (1973) and Arakawa and Schubert (1974), the moist static energy $h_u(\lambda,p)$ within each cumulus updraft is given by integrating (12a) from cloud base $p_B(\lambda)$ to the level p:

$$h_u(\lambda,p)=\frac{1}{\eta_u(\lambda,p)}\left[h_u(\lambda,p_B)+\int_p^{p_B(\lambda)}\eta_u(\lambda,p)\frac{\lambda H}{p}\tilde{h}dp\right]. \tag{13}$$

We assume that each cloud entrains through its entire depth up to some level $p_D(\lambda)$ where it loses its buoyancy and detrains. At this level the cloud virtual temperature, $T_{vc}\equiv T_c(1+0.608q_c-q_l)$, equals the virtual temperature of the environment, where q_l is the cloud condensate mixing ratio and the subscript c refers to cloud values. This condition, when combined with the two approximations (see Arakawa and Schubert)

$$T_c-\tilde{T}\approx\frac{1}{c_p}\frac{1}{1+\gamma}(h_c-\tilde{h}^*), \tag{14a}$$

$$q_c-\tilde{q}^*\approx\frac{1}{L}\frac{\gamma}{1+\gamma}(h_c-\tilde{h}^*), \tag{14b}$$

leads to the following expression for the cloud moist static energy at the detrainment level p_D:

$$h_u(p_D)\approx\tilde{h}^*-\frac{L\mu(1+\gamma)}{1+0.608\mu\gamma}[0.608(\tilde{q}^*-\tilde{q})-q_l], \tag{15}$$

where $\tilde{q}^*$ is the saturation mixing ratio, $\tilde{h}^*$ is the saturation moist static energy, $\gamma\equiv L/c_p(\partial\tilde{q}^*/\partial T)_p$ and $\mu\equiv c_p\tilde{T}/L$. The second term on the right-hand side of (15) is small compared to h^*, which has led to its neglect in the diagnostic studies of Yanai *et al.* (1973) and Ogura and Cho. In the diagnostic study of Nitta (1975), Eq. (15) is used excluding the contribution due to the condensate mixing ratio.

Using standard radiosonde observations of temperature and relative humidity and assuming a cloud-base value of the moist static energy, a unique detrainment level or level of vanishing buoyancy, $p_D(\lambda)$, can be determined for each cloud from (13) and (15) provided the environment stratification is conducive to cloud growth (e.g., conditionally unstable). The inverse of this function is defined as $\lambda_D(p)$.

The moist static energy within the downdraft is given by the solution to (12b), i.e., by

$$h_d(\lambda,p)=\frac{1}{\eta_d(\lambda,p)}\left[h_d(\lambda,p_0)+\int_{p_0(\lambda)}^{p}\eta_d(\lambda,p)\frac{\lambda H}{p}\tilde{h}dp\right]. \tag{16}$$

Measurements taken in cumulonimbus downdrafts made during the Thunderstorm Project reveal that most downdrafts from cumulonimbus clouds in Ohio and Florida originate around the 25 000 ft (400 mb) level with detrainment or spreading of the downdraft air taking place predominantly below cloud-base level. Braham (1952) reports the average surface divergent layer depth to be about 800 m for Florida cumulonimbi. In conformity with these findings it is assumed in the downdraft model that detrainment takes place only in the region below cloud base. Aircraft flights reported by Malkus (1954) through shallow, nonprecipitating tropical cumuli indicate that the in-cloud downdrafts do not extend below cloud base. It may be necessary to modify the plume model for these smaller clouds accordingly. These observations and others mentioned later will be used to specify $p_0(\lambda)$ and $h_d(\lambda,p_0)$ so that (16) can be solved for properties of the downdraft for each cloud type.

c. *Cumulus and synoptic-scale interaction*

In the convective disturbances that are a part of this study, it is assumed that the fractional area occupied by active cumulus towers is $\ll 1$. Extending the formulation of Ogura and Cho (1973) to include the contribution due to cumulus-scale downdrafts, the large-scale average of any quantity α at any level p can be written as

$$\bar{\alpha}(p)=\int_0^{\lambda_D(p)}\alpha_u(\lambda,p)\sigma_u(\lambda)d\lambda+\int_0^{\lambda_D(p)}\alpha_d(\lambda,p)\sigma_d(\lambda)d\lambda+[1-\sigma_u(p)-\sigma_d(p)]\tilde{\alpha}, \tag{17}$$

where α_u, α_d, $\bar{\alpha}$ are the values of α in the updraft, downdraft and environment; $\sigma(\lambda)d\lambda$ represents the fractional area occupied by clouds having entrainment rates in the interval $\lambda-d\lambda/2$ to $\lambda+d\lambda/2$; and $\sigma_u(p)$, $\sigma_d(p)$ represents the total fractional area occupied by updrafts, downdrafts at level p. Using the definitions $m_u(\lambda,p)\equiv-\sigma_u(\lambda)\omega_u(\lambda,p)$ and $m_d(\lambda,p)\equiv-\sigma_d(\lambda)\omega_d(\lambda,p)$, the eddy flux of any quantity α is given by

$$\overline{\alpha'\omega'}=-\int_0^{\lambda_D(p)} m_u(\lambda,p)(\alpha_u-\bar{\alpha})d\lambda -\int_0^{\lambda_D(p)} m_d(\lambda,p)(\alpha_d-\bar{\alpha})d\lambda, \quad (18)$$

where we have used the approximation $\tilde{\alpha}\approx\bar{\alpha}$, which is valid for $\alpha=q$, s and h (e.g., Yanai *et al.*, 1973).

By incorporating cumulus downdrafts into the diagnostic model, two processes that contribute to the total large-scale evaporation $\bar{e}$ can be treated separately: 1) the evaporation $\bar{e}_u$ of liquid water detrained from updrafts, and 2) the evaporation $\bar{e}_d$ of falling precipitation in downdrafts. Thus, we can alternately write (2) in the form

$$-\frac{Q_2}{L}=-\bar{c}+\bar{e}_u+\bar{e}_d-\frac{\partial}{\partial p}(\overline{q'\omega'}). \quad (19)$$

Within the downdrafts evaporation is a source of water vapor as expressed in the water vapor continuity equation for the downdraft:

$$\frac{\partial}{\partial p}(m_d q_d)-\tilde{q}\frac{\partial m_d}{\partial p}=-e_d(\lambda,p). \quad (20)$$

The condensation rate in the updraft is determined from

$$\frac{\partial}{\partial p}(m_u q_u)-\tilde{q}\frac{\partial m_u}{\partial p}=c(\lambda,p). \quad (21)$$

Using (18) with $\alpha=q$, Eqs. (19), (20) (21), and the definitions

$$\bar{c}(p)\equiv\int_0^{\lambda_D(p)} c(\lambda,p)d\lambda, \quad \bar{e}_d(p)\equiv\int_0^{\lambda_D(p)} e_d(\lambda,p)d\lambda,$$

it can be shown (Johnson, 1975) that

$$-\frac{Q_2}{L}=-(M_u+M_d)\frac{\partial\tilde{q}}{\partial p}+\bar{e}_u+\delta[q_u(\lambda_D,p)-\tilde{q}], \quad (22)$$

where $\delta(p)\equiv m_u(\lambda_D,p)d\lambda_D/dp$ is the detrainment rate.

The counterpart of (22) for the no-downdraft case ($M_d=0$) was derived originally by Arakawa (1971), Ooyama (1971) and Yanai (1971). The apparent moisture sink Q_2, as (22) shows, is produced by $M_u\partial\tilde{q}/\partial p$, which represents environmental sinking, compensating cumulus updraft mass flux, and is reduced by the detrainment of water vapor $\delta(q_u-\tilde{q})$ and the evaporation of liquid water $\bar{e}_u$ from cumulus updrafts. The new effect which has been introduced by inclusion of cumulus downdrafts is represented by the term $M_d\partial\tilde{q}/\partial p$. Since $M_d<0$, this term contributes as a moisture source. It can be interpreted as a contribution to environmental lifting and, hence, moistening in response to cumulus downdraft mass flux. Recalling that $M_c\equiv M_u+M_d$ is the *net* cumulus mass flux, we see that the degree to which the large scale is depleted of moisture by convective activity depends critically on the relative intensities of updrafts and downdrafts.

By repeating the above procedure leading to (22) with some slight modifications, an analogous expression can be derived for the large-scale heat budget. Using (18) with $\alpha=s$ and Eqs. (12a, b), (20) and (21), Eq. (1) takes the form

$$Q_1-Q_R=-(M_u+M_d)\frac{\partial\tilde{s}}{\partial p}-L\bar{e}_u+\delta[s_u(\lambda_D,p)-\tilde{s}]. \quad (23)$$

The apparent heat source (minus radiative heating) is produced by environmental sinking compensating the upward cumulus mass flux and detrainment of heat from cloud tops. Large-scale cooling results from the evaporation of detrained liquid water from cumulus updrafts and induced environmental lifting caused by cumulus downdrafts.

Summing (22) and (23) yields

$$Q_1-Q_2-Q_R=\delta[h_u(\lambda_D,p)-\tilde{h}]-(M_u+M_d)\frac{\partial\tilde{h}}{\partial p}. \quad (24)$$

From this expression it is seen that the large-scale moist static energy is affected by three basic processes: radiative heating, detrainment of excess moist static energy from clouds, and environmental sinking or lifting compensating the *net* cumulus mass flux. Since in the standard tropical atmosphere $\partial h/\partial p>0$ in the lower troposphere and $\partial\tilde{h}/\partial p<0$ in the upper troposphere, the downdraft term has the effect of increasing $\tilde{h}$ in the lower troposphere and decreasing $\tilde{h}$ in the upper troposphere. Ogura and Cho (1973) and Nitta (1975) have used (24), excluding the downdraft term, to diagnose properties of cumulus populations from synoptic-scale observations. Writing (24) in the expanded form

$$Q_1-Q_2-Q_R=m_B(\lambda)\eta_u(\lambda_D,p)\frac{d\lambda_D}{dp}[h_u(\lambda_D,p)-\tilde{h}] -\frac{\partial\tilde{h}}{\partial p}\left[\int_0^{\lambda_D(p)} m_B(\lambda)\eta_u(\lambda,p)d\lambda +\int_0^{\lambda_D(p)} m_0(\lambda)\eta_d(\lambda,p)d\lambda\right], \quad (25)$$

we see that if $p_0(\lambda)$ in $\eta_d(\lambda,p)$ is specified, then (25) is an integral equation containing two unknown functions $m_B(\lambda)$ and $m_0(\lambda)$. All other quantities in (25) can be computed using observations of synoptic-scale thermodynamic variables with the previously stated cloud-model assumptions.

As it stands (25) cannot be solved. It is proposed that a new function $\epsilon(\lambda)$ can be meaningfully specified, where

$$\epsilon(\lambda)\equiv\frac{m_0(\lambda)}{m_B(\lambda)}. \tag{26}$$

Having made this assumption, (25) can be rewritten as

$$Q_1-Q_2-Q_R=m_B(\lambda)\eta_u(\lambda_D,p)\frac{d\lambda_D}{dp}[h_u(\lambda_D,p)-\tilde{h}] -\frac{\partial\tilde{h}}{\partial p}\left\{\int_0^{\lambda_D(p)} m_B(\lambda)[\eta_u(\lambda,p)+\epsilon(\lambda)\eta_d(\lambda,p)]d\lambda\right\}. \tag{27}$$

Eq. (27) is now a Volterra integral equation of the second kind for the single unknown function $m_B(\lambda)$, provided that $\epsilon(\lambda)$ and $p_0(\lambda)$ are known. No attempts have been made to find an analytical solution to (27); rather, a numerical approach has been adopted.

It is necessary, of course, to provide a proper physical basis for assumption (26). Knowledge of cumulus cloud structure is insufficient at this time to verify this assumption convincingly and establish a precise estimate of $\epsilon(\lambda)$ based on observations. The simplest approximation is to assume that ϵ is a constant for all cloud types. Physically, this means that weak updrafts [$m_B(\lambda)$ small] have correspondingly weak downdrafts [$m_0(\lambda)$ small] and strong updrafts [$m_B(\lambda)$ large] have strong downdrafts [$m_0(\lambda)$ large].

Considering deep cumuli (λ small), it may be possible to draw upon observations to obtain a rough estimate of a typical value of ϵ. We thus rewrite (26) in the form

$$\epsilon(\lambda)\equiv\frac{m_0(\lambda)}{m_B(\lambda)}=\frac{\sigma_d(\lambda)\omega_0(\lambda)}{\sigma_u(\lambda)\omega_B(\lambda)}.$$

Based on Byers and Braham's (1949) cumulonimbus results, we assume that $\sigma_d(\lambda)\approx 0.8\sigma_u(\lambda)$ and $w_B\approx-\omega_B/\rho g\approx 1$–$2$ m s^{-1}. If $w_0\approx-\omega_0/\rho g\approx-0.5$ m s^{-1} as Betts' (1973a) data indicate, then $\epsilon\approx-0.2$ to -0.4. In the work carried out here an optimum value for ϵ is selected based on 1) comparison of model-computed precipitation with observed rainfall and 2) an examination of the subcloud-layer moisture budget.

In the following analysis an expression is derived for the total precipitation rate $P\equiv C-E_u-E_d$ given by the diagnostic model, where C is the total condensation rate, E_u the total evaporation from cumulus updrafts and E_d the total evaporation within cumulus downdrafts. Integrating (21) from $\lambda=0$ to $\lambda=\lambda_D(p)$ and then from cloud base $p=p_B$ to the top of the tallest cloud, $p=p_T$, in units of mass per unit area per unit time, we find

$$C=\frac{M_u(p_B)}{g}[q_u(p_B)-\tilde{q}(p_B)] -\frac{1}{g}\int_0^{\lambda_D(p_B)} m_u(\lambda,p_D)[q_u(\lambda,p_D)-\tilde{q}]d\lambda +\frac{1}{g}\int_{p_T}^{p_B} M_u\frac{\partial\tilde{q}}{\partial p}dp, \tag{28}$$

where it has been assumed that the updraft mixing ratio at cloud base, $q_u(p_B)$, is independent of λ. The first term on the right-hand side of (28) represents the water vapor flux at cloud base due to all updrafts; the second, the amount of water vapor detrained by all updrafts, contributing negatively to C; and the third, the effects of environmental subsidence compensating the cumulus updraft mass flux M_u.

Repeating the above integrations, this time on (20), we obtain

$$E_d=-\frac{1}{g}\int_0^{\lambda_D(p_B)} m_d(\lambda,p_B)[q_d(\lambda,p_B)-\tilde{q}(p_B)]d\lambda -\frac{1}{g}\int_{p_T}^{p_B} M_d\frac{\partial\tilde{q}}{\partial p}dp. \tag{29}$$

The first term in (29) is a measure of the downward flux of water vapor at cloud base. This term is found to be small in comparison to the second term, which represents the effect of induced environmental lifting in response to the cumulus downdraft mass flux M_d.

The total evaporation from cumulus updrafts is obtained by integrating (22) from p_B to p_T:

$$E_u=\frac{1}{g}\int_{p_T}^{p_B} M_c\frac{\partial\tilde{q}}{\partial p}dp-\frac{1}{g}\int_{p_T}^{p_B}\frac{Q_2}{L}dp -\frac{1}{g}\int_0^{\lambda_D(p_B)} m_u(\lambda,p_D)[q_u(\lambda,p_D)-\tilde{q}]d\lambda. \tag{30}$$

As before, the first term of (30) represents the effects of compensating environmental motions, this time sinking in response to the net cumulus mass flux. The term containing Q_2 is a measure of the large-scale change in the moisture field which changes in direct proportion to E_u.

Combining (28), (29) and (30) yields

$$P=\frac{M_u(p_B)}{g}[q_u(p_B)-\tilde{q}(p_B)]+\frac{1}{g}\int_{p_T}^{p_B}\frac{Q_2}{L}dp +\frac{1}{g}\int_0^{\lambda_D(p_B)} m_d(\lambda,p_B)[q_d(\lambda,p_B)-\tilde{q}(p_B)]d\lambda. \tag{31}$$

Ogura and Cho (1973) derived (31) for the no-downdraft case, where only the first two terms are present.

While it appears that the inclusion of downdrafts in the diagnostic model will modify the precipitation estimates only through the last term in (31), this is not the case. As later results will show, $M_u(p_B)$ itself is changed to such an extent that the term $M_u(q_u-\tilde{q})/g$ is the dominant contributor to the downdraft modification of the computed precipitation P. Eq. (31) provides a means for calibrating model-determined precipitation with observed values, and in so doing, obtaining an optimum selection of ϵ. The results of these comparisons and the subcloud-layer moisture budget in the next section are considered jointly in this selection process.

d. Subcloud-layer moisture budget

In examining the moisture budget for the subcloud layer we formally distinguish the turbulent transport of heat and water vapor by cumulus clouds (and their associated "roots") from that produced by small-scale eddies. Assuming that no condensation takes place below cloud base, the horizontally averaged heat and water vapor equations can be written (using the notation of Ogura and Cho, 1974) as

$$\frac{\partial\bar{s}}{\partial t}+\nabla\cdot\bar{s}\bar{\mathbf{v}}+\frac{\partial}{\partial p}\bar{s}\bar{\omega}=-\frac{\partial}{\partial p}(\overline{s'\omega'})_c+\frac{\partial}{\partial p}F_s+Q_R-L\bar{e}, \quad (32)$$

$$\frac{\partial\bar{q}}{\partial t}+\nabla\cdot\bar{q}\bar{\mathbf{v}}+\frac{\partial}{\partial p}\bar{q}\bar{\omega}=-\frac{\partial}{\partial p}(\overline{q'\omega'})_c+\frac{\partial}{\partial p}F_q+\bar{e}, \quad (33)$$

where $(\overline{s'\omega'})_c$ and $(\overline{q'\omega'})_c$ represent the cumulus fluxes of heat and moisture due to cloud roots, F_s and F_q are the small-scale turbulent fluxes of heat and moisture and, as before, $\bar{e}$ represents precipitation evaporation. It is assumed in accordance with observations that in areas not occupied by clouds a thin transition layer exists between the mixed layer and cloud base at p_B (e.g., Malkus, 1960). Integrating (33) from the surface p_s to cloud base p_B, which is assumed constant in time and horizontally uniform, leads to

$$\Delta p\left[\frac{\partial\bar{q}_m}{\partial t}+(\nabla\cdot\bar{q}\bar{\mathbf{v}})_m\right]-\bar{q}_B\bar{\omega}_B=(\overline{q'\omega'})_B+F_{q\,\mathrm{sfc}}+\bar{e}_m\Delta p, \quad (34)$$

where the subscripts B and sfc refer to cloud base and surface values, $\Delta p=p_s-p_B$,

$$(\ )_m\equiv\frac{1}{\Delta p}\int_{p_B}^{p_s}(\ )dp,$$

and $F_{q\,\mathrm{sfc}}/g$ represents the surface evaporation. The turbulent eddy flux of water vapor atop the transition layer, F_{qB}, is assumed to vanish. Using (18) we can rewrite (34) in the form

$$\Delta p\left[\frac{\partial\bar{q}_m}{\partial t}+(\nabla\cdot\bar{q}\bar{\mathbf{v}})_m\right]-\bar{q}_B\bar{\omega}_B=-M_{uB}(q_{uB}-\tilde{q}_B)$$
$$-\int_0^{\lambda_D(p_B)}m_d(\lambda,p_B)[q_d(\lambda,p_B)-\tilde{q}_B]d\lambda+F_{q\mathrm{sfc}}+\bar{e}_m\Delta p.$$

Recalling that

$$\tilde{M}\equiv-\bar{\omega}=M_u+M_d+\tilde{M},\quad M_d=\int_0^{\lambda_D(p_B)}m_d(\lambda,p)d\lambda$$

and $\tilde{q}\approx\bar{q}$, then

$$\Delta p\frac{\partial\bar{q}_m}{\partial t}+\Delta p(\nabla\cdot\bar{q}\bar{\mathbf{v}})_m+\tilde{M}_B\bar{q}_B+M_{uB}q_{uB}$$
$$+\int_0^{\lambda_D(p_B)}m_d(\lambda,p_B)q_d(\lambda,p_B)d\lambda$$
$$-F_{q\mathrm{sfc}}-\bar{e}_m\Delta p=0. \quad (35)$$

The terms in (35) represent the following processes affecting the subcloud layer water vapor content in the order they appear: storage, convergence, environmental or between-cloud transport, cumulus updraft transport, cumulus downdraft transport, surface evaporation and rainfall evaporation. Transport of water vapor by cumulus downdrafts (note $m_d<0$) has not been previously considered in budget studies of the subcloud layer. This contribution, as results of application of the diagnostic model show (Section 3), is an important one that must be included in the budget analysis when precipitating clouds are present. Appearing in the downdraft term is the water vapor content $q_d(\lambda,p_B)$ of the individual cumuli at cloud base. Though the value of this term depends on the buoyancy assumption at the downdraft originating level, it will be seen that the sensitivity to whatever assumption is made, within reasonable bounds, is not great enough to alter its magnitude by more than a few percent. Estimate of evaporation of rainfall in the subcloud layer is made in this study by using results of the cloud-layer model. Evaporation within downdrafts at cloud base, $\bar{e}_d(p_B)$, computed from this model is assumed to be equivalent to the evaporation rate $\bar{e}_m$ that the subcloud layer experiences.

One further remark about (35) is necessary. Both $\tilde{M}$ and M_{uB} are influenced by the cumulus downdraft mass flux. Correspondingly, the third and fourth terms, in addition to the fifth and seventh, will be modified when the effects of downdrafts are included in the water vapor budget analysis of the subcloud layer.

3. Model application: Western Pacific results

Reed and Recker (1971) have presented the detailed structure of an average easterly wave obtained by compositing a series of 18 tropical wave disturbances that

traversed the Marshall Islands area of the western Pacific during a 90-day period (July–September, 1967). Cho and Ogura (1974) have applied the diagnostic model developed by Ogura and Cho (1973) to the Reed and Recker data set. They reached the general conclusion that a bimodal population of cumulus clouds, i.e., abundant deep types and shallow types, exists during disturbed conditions, whereas predominately shallow-type cumuli exist during undisturbed conditions. Reed and Recker, using a single deep-cloud model containing an unsaturated downdraft, have shown that mass transport in cumulus downdrafts contributes substantially to the total convective mass transport in the trough region of the composite wave. In this section we will show that by including the effects of convective-scale downdrafts, the conclusion of Cho and Ogura for the convective region of the wave is altered; specifically, that the contribution to the total cumulus mass flux by shallow clouds has been overestimated.

The determination of $\lambda_D(p)$ requires, in addition to the basic thermodynamic variables, specification of the moist static energy at cloud base, $h_u(\lambda,p_B)$, and the cloud base height $p_B(\lambda)$. In this study it is assumed that the virtual temperature excess at cloud base and cloud top are zero. Thus, $h_u(\lambda,p_B)$ is given by (15) with $q_l=0$. Values of the liquid water content that are used to evaluate (15) at the detrainment level for each cloud have been taken from measurements summarized by Byers (1965) in his Fig. 6.5. These values increase from zero at cloud base to about 1 g kg^{-1} at 600 mb, decreasing to about 0.5 g kg^{-1} at 100 mb.

Specification of the buoyancy condition at the downdraft originating level $h_d(\lambda,p_0)$ is complicated by the fact that the structure and intensity of downdrafts from cumulonimbus clouds are frequently dependent upon the environmental stratification of temperature, moisture and wind. It has been proposed that downdrafts from intense, well-organized thunderstorms are strongly influenced by the injection of air at mid-tropospheric levels having low moist static energy (Newton, 1966; Zipser, 1969). It is noted, however, that the solution of (27) for $m_B(\lambda)$ is independent of whatever value of $h_d(\lambda,p_0)$ is selected, although it does depend on $p_0(\lambda)$. The subcloud-layer budget will be influenced by the selection of $h_d(\lambda,p_0)$, but only in a minor way.

In an attempt to determine the sensitivity of the downdraft structure to the buoyancy condition at the downdraft originating level, two different assumptions have been tested:

(i) $h_d(\lambda,p_0)=\tilde{h}^*(p_0)$

(ii) $h_d(\lambda,p_0)=0.5[\tilde{h}^*(p_0)+h_u(\lambda,p_0)]$.

Consider first the meaning of these two assumptions for deep cumulonimbi. If downdrafts from these clouds originate in the upper troposphere, where roughly speaking, $\tilde{h}^*\approx\tilde{h}$, then assumption (i) corresponds to the situation where the air at the downdraft originating level is predominantly evaporation-cooled environmental air. The second assumption would imply that downdraft air at its originating level is approximately an equal mixture of environmental air and air from the updraft. This corresponds to the situation where liquid water drag accounts for the negative buoyancy and the downdraft air at this high level is warmer than the environment [e.g., as in model results of Wilhelmson (1974) and Miller and Pearce (1974)]. As one proceeds to shallower clouds, $h_u(\lambda,p_0)\rightarrow h^*(p_0)$, and assumptions (i) and (ii) become approximately the same. When one of these conditions is imposed, $h_d(\lambda,p)$ can be computed from (16).

We next assume that downdrafts originate at a level above cloud base given by a certain fraction β of the pressure-depth of the corresponding updraft, that is, we assume (where we have chosen $p_B=950$ mb for all cloud types)

$$p_0(\lambda)=p_B-\beta[p_B-p_D(\lambda)]. \tag{36}$$

For clouds which have tops at 200 mb and bases at 950 mb, $\beta=0.75$ gives $p_0\approx390$ mb (24 000 ft). This compares well with the observations of thunderstorm downdraft-originating levels reported by Braham (1952) and Betts (1973a). Experiment with different values of β have been carried out; however, based on the above calculation for deep clouds, $\beta=0.75$ is considered to be the preferred value. Verification of (36) for shallower clouds is difficult due to the lack of measurements of $p_0(\lambda)$ for small clouds.

The function $\lambda_D(p)$ was computed from (13) for the wave-trough region using an iterative scheme described in Johnson (1975). $\lambda_D(p)$ [not shown] increases monotonically from 0 at 120 mb to 1.8 km^{-1} at 950 mb. In Fig. 3 the temperature and mixing ratio in individual updrafts and downdrafts are shown for two different entrainment rates, $\lambda=0.05$, 0.25 km^{-1}; $h_d(\lambda,p_0)=h^*(p_0)$ and $\beta=0.75$. These values have been computed assuming that the downdraft is saturated. Although work such as that of Kamburova and Ludlam (1966) has demonstrated that evaporation of raindrops normally does not proceed at a sufficient rate to maintain saturation in the downdraft, a correction for subsaturation has not been applied, since direct measurements of the degree of subsaturation in tropical cumulonimbus downdrafts are lacking. The deep cumulonimbus updraft has peak temperature and mixing ratio excesses of $\sim$4°C and 5 g kg^{-1}. Note that in the lowest 25 mb of the updrafts the in-cloud temperature is lower than that in the environment. In this region the updrafts owe their buoyancy solely to their elevated moisture content. Downdrafts from the deep convective cells are characteristically colder than the environment below 600 mb. The two downdrafts shown have temperature deficits at cloud base of ~-3°C and mixing ratio deficits of ~-0.7 g kg^{-1}.

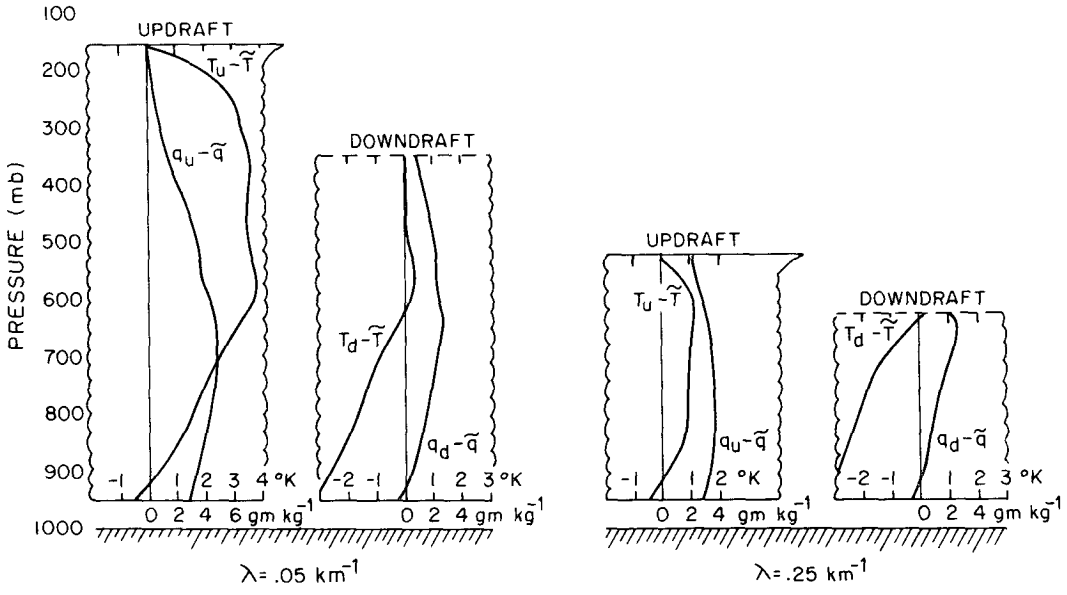

FIG. 3. Cloud updraft and downdraft temperature and mixing ratio excesses assuming $h_d(\lambda,p_0)=h^*(p_0)$ and $\beta=0.75$.

For the purposes of determining the influence of downdrafts on the subcloud layer, it is important to examine the sensitivity of the downdraft temperature and mixing-ratio excesses at cloud base to the originating-level, moist static energy assumption. The results of the examination for assumptions (i) and (ii) are shown in Fig. 4, where (14a, b) and (16) have been used to compute $(T_d-T)_{p_B}$ and $(q_d-\tilde{q})_{p_B}$. We see that these values are relatively insensitive to our choice of originating-level condition for almost all cloud sizes. Also note that nearly all cumuli with $\lambda\lesssim 0.4$ (tops above 600 mb) produce downdrafts which are colder and have a lower mixing ratio than the environment at cloud base.

In order to solve (27) for properties of the cumulus populations, Q_1, Q_2 and Q_R must be determined from large-scale observations. Radiosonde data for the composite wave have been assigned by Reed and Recker to eight different categories. Category 4 corresponds to the trough axis, 8 to the ridge axis, 2 to the axis of maximum northerly flow in the lower troposphere and 6 to the axis of maximum southerly flow. Categories 1, 3, 5, 7 are intermediates to these. Reed and Johnson (1974a) computed Q_1 and Q_2 for the entire composite wave, discovering in the process that there exists a pronounced variation in the observed Q_2 fields in the trough region, categories 3, 4, 5 (see Fig. 5). Acknowledging inaccuracies in the observational data, it was felt appropriate to apply a smoothing (over category) to Q_1 and Q_2. A 3-point filter was used with a central weight of 0.50 and outer weights of 0.25. Fig. 5 (right) shows the smoothed profiles of Q_1 and Q_2 for the wave-

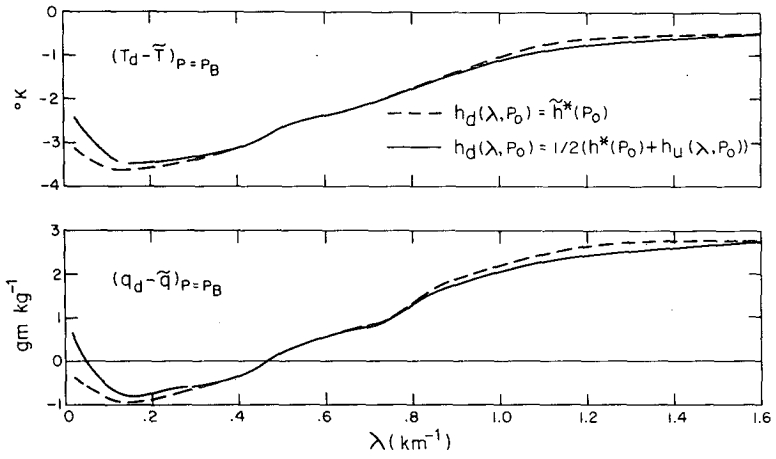

FIG. 4. Downdraft temperature and mixing ratio excesses/deficits at cloud base for the two different assumptions of $h_d(\lambda,p_0)$ and for $\beta=0.75$.

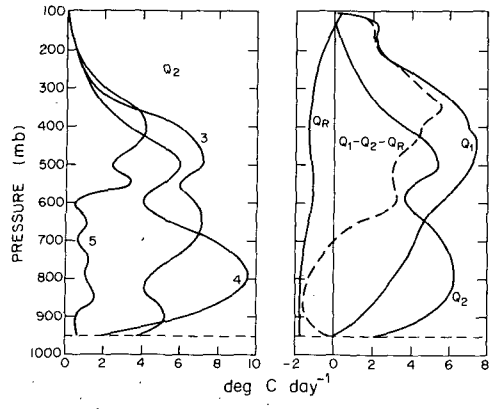

FIG. 5. Apparent moisture sink for categories 3, 4, 5 (left). Apparent heat source, moisture sink, net radiative heating rate and their sum for average wave trough are shown at right.

trough region. The radiative heating profile is taken from Dopplick (1972).

The role of convective downdrafts has been determined by solving (27) employing realistic estimates of ϵ and β. Recall that ϵ measures the relative magnitude of the downdraft compared to the updraft and β measures the fraction of the pressure-depth of the updraft occupied by the downdraft. Solutions have been obtained numerically using standard methods for solving Volterra integral equations of the second kind (Delves and Walsh, 1974) with all integrals being evaluated by the trapezoidal method. Special care is necessary with the downdraft term because the limit of integration in η_d, the level p_0, is a function of cloud entrainment rate λ. A resolution in λ of 0.025 km^{-1} is chosen, meaning that about 40 clouds are used to depict the entire population of cumulus clouds. Because of the character of $\lambda_D(p)$, however, only one-fourth of this total turn out to have tops above the 500 mb level.

The results of the integrations for the wave-trough position are presented in Fig. 6. The cloud-base mass flux distribution function $m_B(p)$, defined as $m_B(\lambda)d\lambda_D/dp$, is shown for the no-downdraft case, $\epsilon=0$, and for several downdraft intensities given by $\epsilon=-0.2$ with $\beta=0.5$, 0.75 and $\epsilon=-0.4$ with $\beta=0.75$. Without downdrafts it is seen that there is a relatively large contribution to the total cloud-base mass flux by shallow cumuli (those having tops below ~700 mb). As the downdraft intensity is increased, however, the mass flux contribution by shallow cumuli is reduced. Negative values of $m_B(p)$ appear in the lower troposphere for $|\epsilon|\gtrsim 0.5$. Thus, we conclude that the value of $|\epsilon|$ that gives a proper assessment of the role of downdrafts lies in the range 0.0 to 0.5. An optimum value for ϵ will be selected based on precipitation calibration and examination of the subcloud-layer moisture budget.

Also in Fig. 6 the cumulus mass fluxes in updrafts and downdrafts are shown for $\epsilon=0$, -0.2 and $\beta=0.5$, 0.75. Downdraft mass fluxes for $\epsilon=-0.2$ increase downward from zero in the mid-troposphere to approximately one-fourth the magnitude of the updraft mass fluxes at cloud base. The updraft mass flux M_u is reduced approximately 10–15% below 700 mb when $|\epsilon|$ is increased to 0.2. We compare these results with computations made by Reed and Recker (1971) of M_u, M_d for the wave troughs that are based on a single deep-cloud model containing an unsaturated downdraft. Note that there is reasonable agreement for $\epsilon=-0.2$, $\beta=0.75$.

To assist in the determination of an optimum value of ϵ, the total condensation, updraft evaporation, downdraft evaporation (assuming a saturated downdraft) and precipitation have been computed from the cloud layer model for different values of ϵ. Fig. 7 shows the results of these computations for $\beta=0.5$, 0.75 and $h_d(\lambda,p_0)=\tilde{h}^*(p_0)$. We define precipitation rate P_g at the ground as P minus precipitation evaporation in the subcloud layer, where P is given by (31) and evaporation in the subcloud layer has been computed by

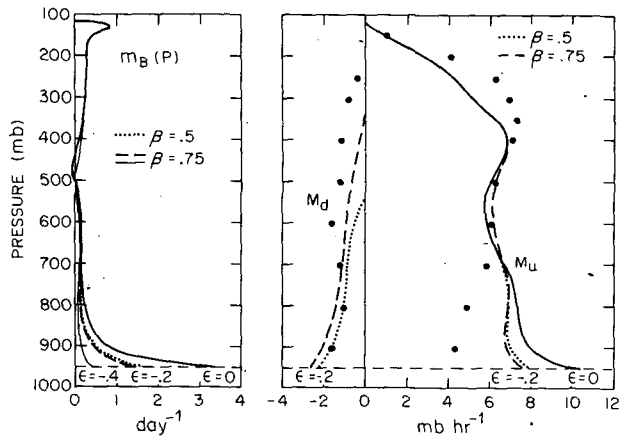

FIG. 6. Cloud-base mass flux distribution function $m_B(p) \equiv m_B(\lambda)d\lambda_D/dp$ (left) for $\epsilon=-0.2$ ($\beta=0.5$, 0.75) and $\epsilon=-0.4$ ($\beta=0.75$), and updraft, downdraft mass fluxes (right) for $\epsilon=0$, -0.2 ($\beta=0.5$, 0.75). Large dots are from Reed and Recker, Table 3.

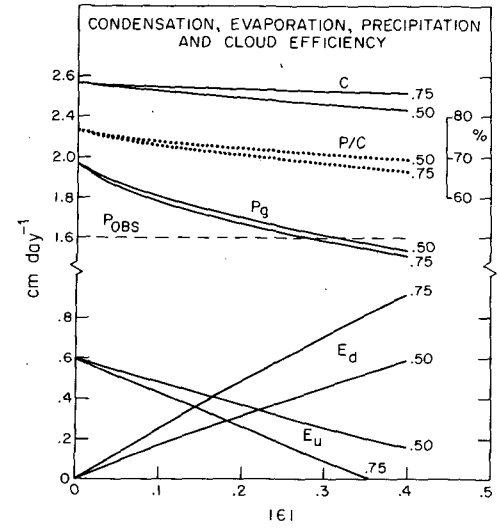

FIG. 7. Condensation, evaporation, precipitation and cloud efficiency from cloud-layer budget as a function of $|\epsilon|$ for wave trough. Numbers at end of lines are values of β.

assuming that the rainfall evaporation throughout this layer is equal to the rate at cloud base obtained from (20). Since surface observations within thunderstorm downdrafts normally show the air to be subsaturated, this rate represents an upper limit to the subcloud-layer evaporation. Indicated on this diagram is the observed precipitation rate P_{OBS}, for the mean wave trough, 1.61 cm day^{-1}. The curve representing the computed value of P_g intersects P_{OBS} at $\epsilon=-0.26$. The same value is obtained (within 1%) if we alternatively assume $h_d(\lambda,p_0)=0.5[h_u(\lambda,p_0)+h^*(p_0)]$.

The total evaporation in updrafts and downdrafts is seen in Fig. 7 to be quite sensitive to β. Downdrafts which start from higher levels ($\beta=0.75$) are seen to evaporate substantially more liquid water than shorter ones ($\beta=0.5$) for the same ϵ. The total condensation and precipitation are not so dependent on β, however, because they are largely determined by the updraft mass flux M_u which is relatively insensitive to β (Fig. 6). For $\epsilon=-0.26$ and $\beta=0.75$, total evaporation in downdrafts is about four times that from updrafts. Cloud efficiencies, defined as the ratio of precipitation (at cloud base) to total condensation, have also been computed. The values here ($\sim$70%) are larger than those computed by Braham (1952) for Ohio and Florida thunderstorms and Betts (1973a) for Venezuelan thunderstorms, and slightly less than those given by Yanai *et al.* for ITCZ convection in the Marshall Islands region.

In view of the uncertainties involved in the determination of an optimum value of ϵ, it has been decided to use the conservative value $\epsilon=-0.2$ in illustrating the important role of cumulus downdrafts in the heat and moisture budgets for the cloud layer. As mentioned earlier, the net cumulus mass flux and environmental sinking in the lower troposphere are reduced when downdrafts are included in the model. Fig. 8 shows that for $\epsilon=-0.2$, $\beta=0.75$, $M_c(p_B)$ and $\tilde{M}(p_B)$ are nearly one-half of the corresponding values for the no-downdraft case. Because of this reduction in environmental sinking in the lower troposphere, less evaporation of liquid water from cumulus updrafts is required to keep the atmosphere from drying out. The right-hand diagram in Fig. 8 illustrates this effect. In fact, for $\epsilon=-0.2$, evaporation in downdrafts exceeds evaporation from updrafts at nearly all levels in the troposphere, and in total is about twice that from updrafts (refer to Fig. 7). This description of evaporation processes is certainly more realistic than that provided by the no-downdraft case, where $\bar{e}_u$ is very large in the lower troposphere and $\bar{e}_d=0$. Note that the total evaporation from updrafts and downdrafts is diagnosed not to change significantly as $|\epsilon|$ is increased; it is mainly the partitioning of the evaporation between the two drafts that changes.

Also shown in Fig. 8 are evaporation rates δq_l corresponding to liquid water contents for individual cumuli that were computed using the rainfall parameterization scheme of Ogura and Cho (1973). In accordance with their work, we have assumed in this computation a cloud-base vertical velocity of 1 m s^{-1} and a cloud-droplet-to-hydrometeor conversion constant of 0.004 s^{-1}. For $\epsilon=-0.2$, it is noted that evaporation given by the cloud water budget δq_l and the large-scale moisture balance $\bar{e}_u$ have roughly the same magnitudes.

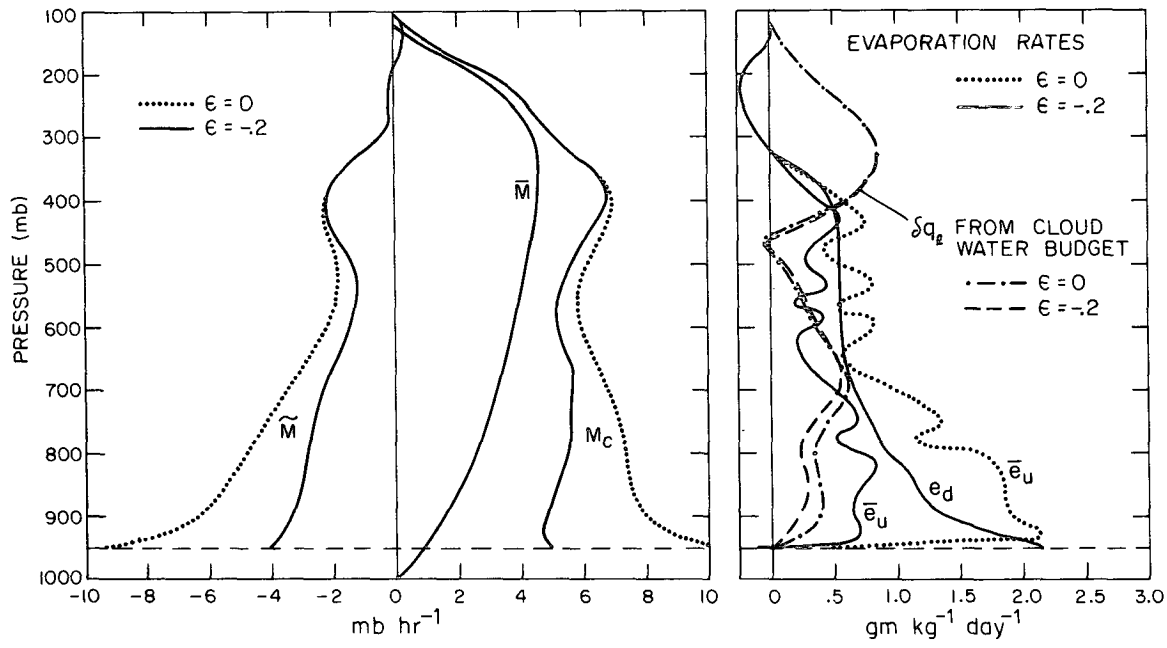

FIG. 8. Net cumulus, and mean and environmental mass fluxes (left) for $\epsilon=0$, -0.2 ($\beta=0.75$), and comparison (right) of updraft detrainment evaporation rate from large-scale water vapor balance ($\bar{e}_u$) with that given by cloud water budget (δq_l) for $\epsilon=0$, -0.2 ($\beta=0.75$). Downdraft evaporation rate $\bar{e}_d$ for $\epsilon=-0.2$, $\beta=0.75$ is also shown.

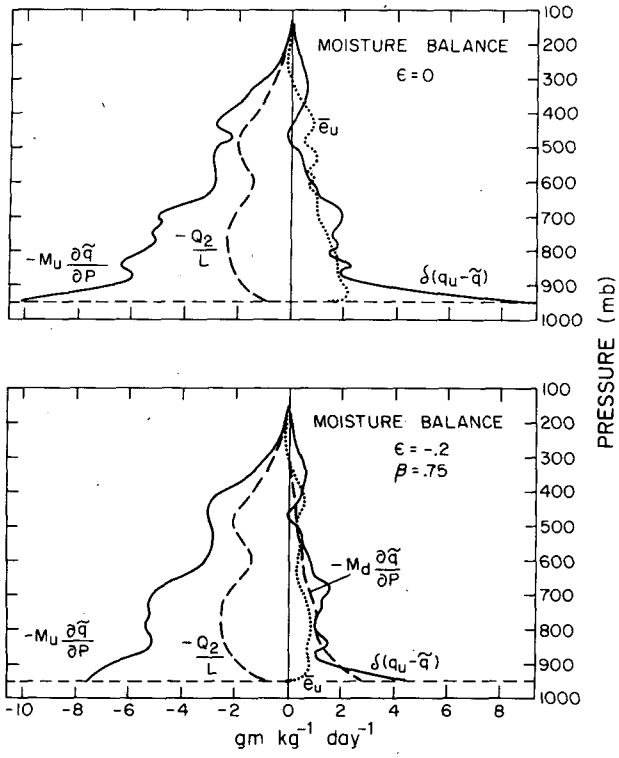

FIG. 9. Processes affecting large-scale water vapor balance for no-downdraft case ($\epsilon=0$) and downdraft case ($\epsilon=-0.2, \beta=0.75$). See text for discussion.

The modification of the large-scale moisture and heat budgets by cumulus downdrafts is illustrated in Figs. 9 and 10. In the case of no downdrafts we see that the apparent moisture sink Q_2 is produced by the drying effects of compensating subsidence outweighing the moistening effects of water vapor and liquid water detrainment (Fig. 9). When downdrafts are included, there is a reduction in the detrainment moistening, but this is offset by moistening produced by environmental lifting compensating the downdrafts. The compensating subsidence is also reduced, but only slightly since M_u changes only slightly (Fig. 6). However, note that the drying due to the net cumulus flux, $M_c\partial\tilde{q}/\partial p$, is reduced substantially. As Yanai *et al.* have previously shown, the apparent heating Q_1-Q_R is largely produced by adiabatic sinking compensating cumulus mass flux, which outweighs the cooling effects of liquid water evaporation from updrafts (Fig. 10). By including the effects of downdrafts, we see a reduction in the evaporation cooling and the introduction of a new effect, adiabatic lifting and cooling in response to the cumulus downdrafts.

We next examine the contribution of downdrafts to the total vertical eddy heat flux F. In Fig. 11 we have presented F and SH_u, LH_u, SH_d, LH_d, the sensible and latent eddy heat fluxes in updrafts and downdrafts, respectively, for $\epsilon=0$ and $\epsilon=-0.2$, $\beta=0.75$ and $h_d(\lambda,p_0)=\tilde{h}^*(p_0)$. These quantities are defined as follows:

$$F\equiv\frac{1}{g}\int_0^{\lambda_D(p)} m_u(\lambda,p)(h_u-\tilde{h})d\lambda + \frac{1}{g}\int_0^{\lambda_D(p)} m_d(\lambda,p)(h_d-\tilde{h})d\lambda$$

$$SH_u\equiv\frac{c_p}{g}\int_0^{\lambda_D(p)} m_u(\lambda,p)(T_u-\tilde{T})d\lambda$$

$$LH_u\equiv\frac{L}{g}\int_0^{\lambda_D(p)} m_u(\lambda,p)(q_u-\tilde{q})d\lambda$$

$$SH_d\equiv\frac{c_p}{g}\int_0^{\lambda_D(p)} m_d(\lambda,p)(T_d-\tilde{T})d\lambda$$

$$LH_d\equiv\frac{L}{g}\int_0^{\lambda_D(p)} m_d(\lambda,p)(q_d-\tilde{q})d\lambda.$$

The latent heat (water vapor) flux in the updraft is the dominant contributor to the total heat flux in the lower troposphere. The latent heat flux in the downdraft is negative, having a peak magnitude near 650 mb decreasing to near zero at cloud base. The sensible heat flux in the downdrafts is positive since they are cooler

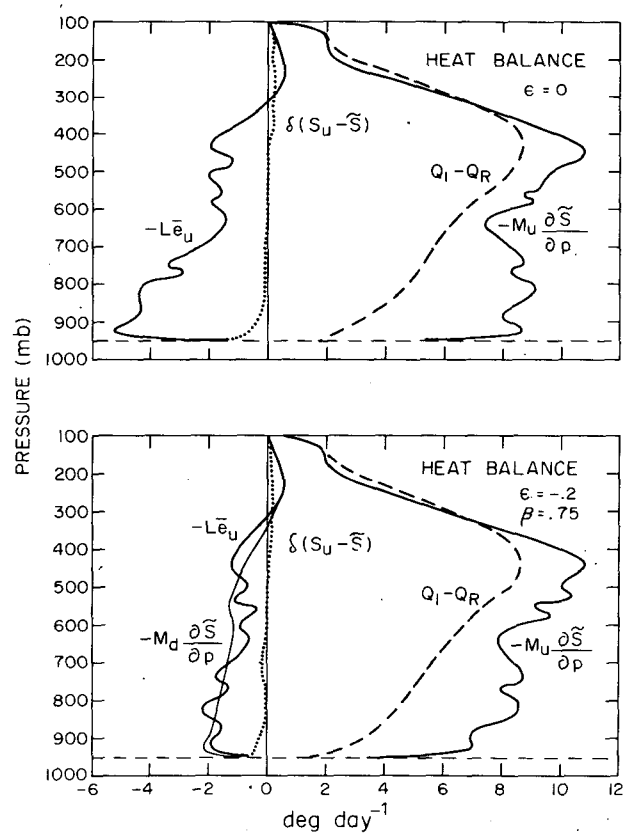

FIG. 10. As in Fig. 9 except for the large-scale heat balance.

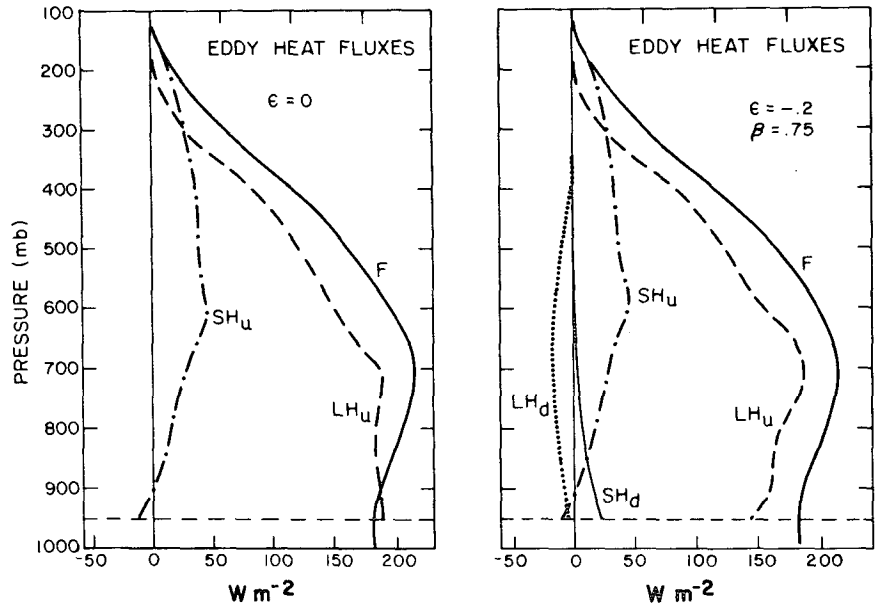

FIG. 11. Sensible, latent and total heat fluxes in updrafts for no-downdraft case ($\epsilon=0$) and in updrafts and downdrafts for $\epsilon=-0.2$, $\beta=0.75$.

than the environment. The contribution of downdrafts to the total convective heat flux for $\epsilon=-0.2$ is, as seen from Fig. 11, under 10%.

It is of interest to compare these heat-flux results with those obtained by Riehl and Malkus (1958) based on a study of the heat balance in the equatorial trough zone. Riehl and Malkus estimated from the residual in their heat budget that the magnitude of the total heat flux in cumulonimbus downdrafts must be 36% of that in updrafts at 500 mb. Their ratio is about four times that determined in this study (Fig. 11). Thus, the results obtained using data from the western Pacific indicate that downdrafts may not play as important a role in the heat transport in the upper troposphere as Riehl and Malkus have previously indicated.

A second estimate of the optimum ϵ for this data set has been achieved by an analysis of the subcloud-layer water vapor budget. The individual terms in (35) have been evaluated as a function of the relative downdraft intensity, given by ϵ. In the computations we have used $\tilde{q}_B=16.5$ g kg^{-1}, $q_{uB}=19.2$ g kg^{-1} and $\Delta p=60$ mb. Evaporation of rainfall in the subcloud layer is obtained by assuming that $\bar{e}_d(p_B)$ given by the cloud layer model is constant in this layer. For the no-downdraft case ($\epsilon=0$) it is seen in Fig. 12 that an imbalance exists, as represented by the residual, that is comparable in size to the surface evaporation and, therefore, probably significant. The between-cloud transport and updraft transport of water vapor are the largest terms of any by at least an order of magnitude as Ogura and Cho (1974) have earlier shown. It is discovered, however, that as $|\epsilon|$ increases, the residual decreases, reaching zero at $\epsilon=-0.20$. In addition, as $|\epsilon|$ increases, the downdraft transport of water vapor increases, reaching a size equivalent to the between-cloud transport when $|\epsilon|$ is slightly greater than 0.20. The addition of water vapor by precipitation evaporation is relatively small compared to the downdraft water vapor transport. We conclude from the results of this section that the neglect of precipitation downdraft in the water vapor budget analysis of the subcloud layer during convectively disturbed conditions leads to a substantial overestimation of the between-cloud or environmental transport of water vapor into this layer.

4. Northern Florida case study

Results from the previous section indicate that, at least in the tropical western Pacific, convective-scale downdrafts contribute in an important way to the modification of the synoptic-scale thermodynamic structure by cumulus clouds. In this section we apply the diagnostic model to a data set from subtropical latitudes, data taken during the passage of a weak tropical depression over northern Florida in September 1969. A post-analysis done by Frank (1970) indicates this depression formed off the northwest coast of Cuba on the 19th and traveled north-northwestward, going ashore over the western tip of the Florida panhandle on the 21st. Very heavy rain fell during a 1–2 day period of this convective system over an extensive area of northern Florida.

Analyses of rainfall rates over the region of interest at 12 h intervals (centered about 0000 and 1200 GMT) during the period of heaviest precipitation have been prepared by Robert Thompson (Fig. 13). Non-hourly as well as hourly observations have been included in each analysis by calibrating the less frequent observa-

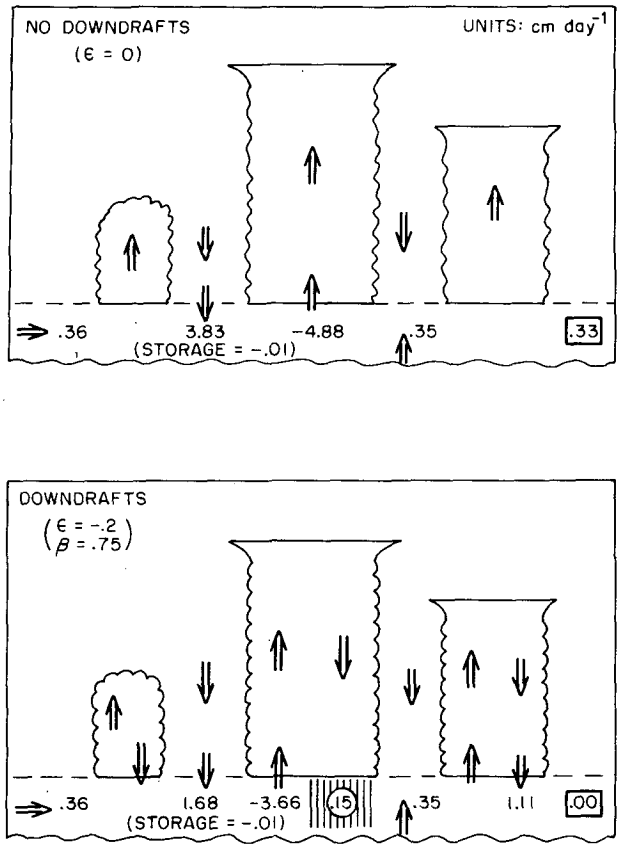

FIG. 12. Schematic of processes affecting subcloud-layer moisture budget for no-downdraft case ($\epsilon=0$) and downdraft case ($\epsilon=-0.2$, $\beta=0.75$). Processes indicated in lower figure from left to right (other than storage) are convergence, environmental sinking, transport into updrafts, rainfall evaporation, surface evaporation and downdraft transport. Residual (cm day^{-1}) is indicated in the small box.

tions with neighboring hourly reporting stations. Peak amounts (>10 cm day^{-1}) occurred over the central portion of northern Florida extending into southern Georgia. The triangle shown in the figure joins the three rawinsonde stations Tampa (TPA) and Valparaiso (VPS), Fla., and Waycross (WAY), Ga. Average rainfall rates for all of the stations within the triangle are shown at each time (in brackets). Approximately 40 stations are included in each average. Although 33% of the area in this triangle extends over the Gulf of Mexico, it is noted from examination of weather radar for this period that the region over water experienced an amount of deep convective activity comparable to that occurring over land in the western portion of the triangle.

From water vapor budget computations (see Appendix) for this triangle of rawinsonde stations, rainfall rates from 0000 GMT on the 19th to 1200 GMT on the 24th have been determined. No corrections were made to the observed relative humidities, as has been necessary in other studies (e.g., Nitta and Esbensen, 1974) due to radiative heating of the hygristor element, since 0000 and 1200 GMT correspond to 1900 and 0700 LT, or times when the sun angle is very low. Evaporation rates were determined by averaging daily pan evaporation measurements from the several National Weather Service sites within this triangular region. The average rate from the 19th to the 24th, 0.25 cm day^{-1}, may be somewhat less than the evaporation rate that existed over the Gulf of Mexico where wind speeds of 10 m s^{-1} or greater occurred during the passage of the depression; however, this water region covers only one-third of the total area. The average of the computed precipitation rates for the period of heaviest observed rainfall corresponding to the four observation times in Fig. 13 is 6.76 cm day^{-1}, 18% greater than the observed average of 5.71 cm day^{-1}. We have composited the four observations for this 36 h period in the application of the diagnostic model rather than trying to carry out computations at each individual time.

In applying the diagnostic model to this case study, we assume that updrafts and downdrafts associated with the cumulonimbus convection occupied only a small fraction (<10%) of the entire area at any particular instant of time. The Apalachicola WSR-57 weather radar PPI data for this time period indicate that the areal coverage of the strong convective cells is indeed small, although precise measurements of areal coverage have not yet been made. For the purposes of calibrating model-computed precipitation with the observed rainfall, we assume that most of the total rainfall was produced by cumulonimbus clouds.

One of the problems in studying a system with so much convective activity is that it is often difficult to obtain atmospheric soundings that accurately represent the cloud environment (Sanders and Paine, 1975). Most of the rainfall over northern Florida occurred in connection with the tropical depression that came ashore from the Gulf of Mexico. Bearing this in mind, we have selected the soundings from TPA and VPS, which are along the Gulf Coast, as being representative of the cumulus environment and have not included those from WAY, which received some minor cooling at low levels due to a weak cold front that extended into southern Georgia on the 20th. For the period 20/1200 GMT to 22/0000 GMT the average soundings for 1) TPA, VPS and WAY and 2) TPA and VPS are compared in Fig. 14. The low-level cooling contributed by WAY in the first average is evident in the profiles of $\tilde{h}^*$. The VPS–TPA averages of $\tilde{h}$ and $\tilde{h}^*$ excluded the sounding for VPS at 21/1200 GMT (indicated by a dotted line) since this observation deviated significantly from the mean for this period.

Fig. 15 shows the results of the computations of Q_1 and Q_2 for this heavy rainfall period. In determining $\bar{\omega}(p)$ we have assumed $\bar{\omega}=0$ at the ground (this region is essentially flat) and at 70 mb. Q_2 was extrapolated from its relatively small value at 300 mb to zero at

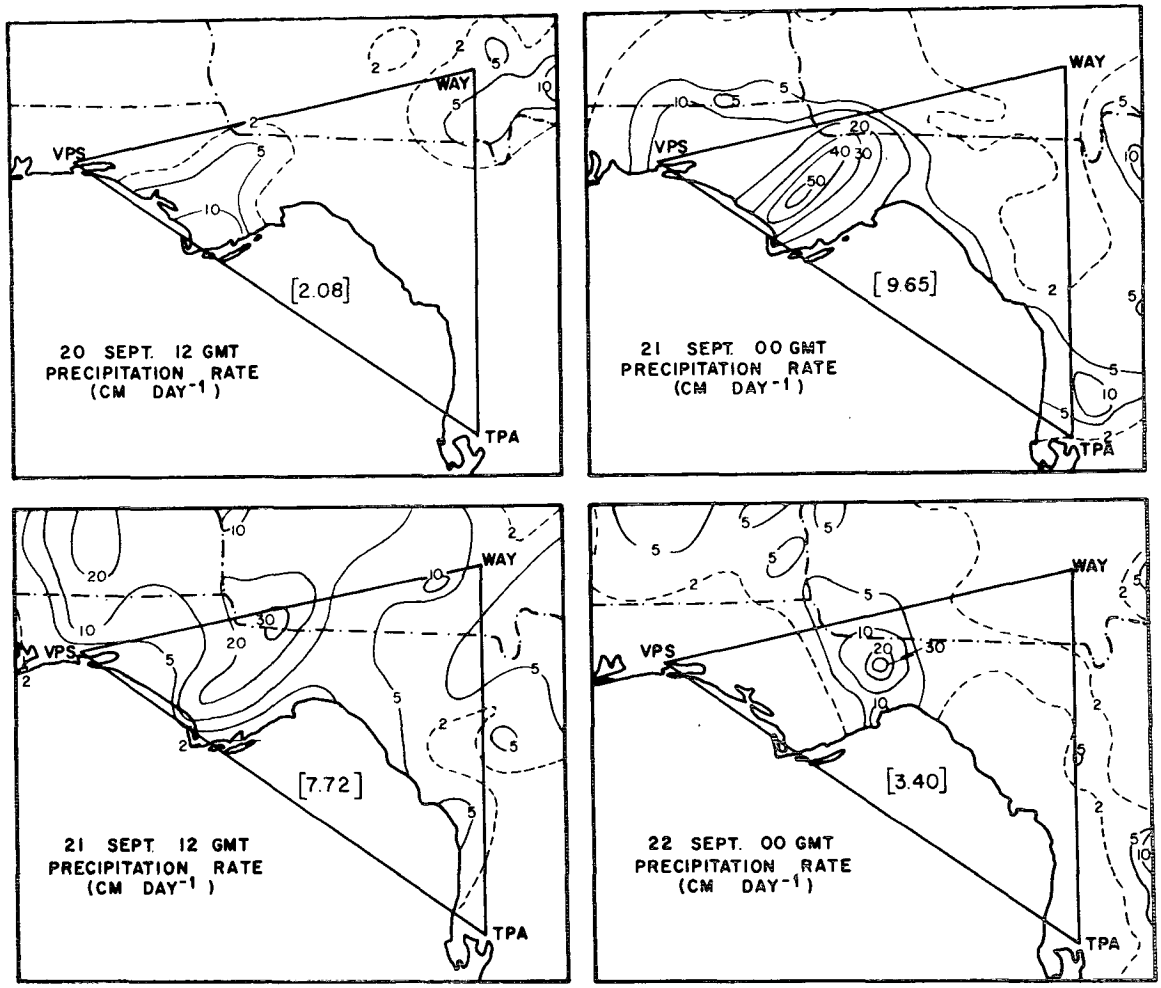

FIG. 13. Precipitation rates (cm day^{-1}) during period of heaviest rainfall in northern Florida case study. Numbers in brackets indicate the average rainfall rates for all stations within the triangle formed by Valparaiso (VPS), Tampa (TPA) and Waycross (WAY).

175 mb, since relative humidity measurements were not available above 300 mb. Included in this figure are the radiative heating rate estimates appropriate for September at 30°N taken from Dopplick (1972).

Remarkably, Q_1 and Q_2 for this northern Florida study (although the individual magnitudes are approximately four times those for the Reed and Recker wave trough) possess features that have striking similarities to the Pacific data set. In particular, Q_2 in both cases has peaks at 800 and 500 mb and a minimum at 600 mb. Additionally, Q_1 has a peak at or slightly above 500 mb in both regions. Yanai *et al.* (1973) have also observed similar features in their analysis of data taken in the Marshall Islands region of the western Pacific. No explanation for the consistently observed minimum in Q_2 at 600 mb has yet been offered. We note, however, from Fig. 14 that since the minimum in $\tilde{h}^*$ occurs near 600 mb, the atmosphere is stable above this level. Possibly then, a relatively large number of clouds detrain their moisture near this level, at least more so than the number which detrain within several hundred millibars above or below. If this is the case, then Q_2, which is a measure of the depletion of moisture due to convection (resulting from environmental sinking), should exhibit a minimum near 600 mb.

In Fig. 16 $m_B(p)$, computed for $\epsilon=0$, -0.2, -0.4 and $\beta=0.75$, is shown. Based on estimates of the lifting condensation level of the surface air and surface visual observations, 950 mb was selected as the cloud base height p_B. Here again we see that a prominent bimodal population of cumulus clouds exists with a peak near 200 mb and a very large low-level maximum when downdrafts are neglected ($\epsilon=0$). Two smaller peaks appear near 425 and 625 mb. As $|\epsilon|$ increases, this low-level maximum is reduced, becoming comparatively small when $\epsilon=-0.4$. It is also noted that several regions of negative values of $m_B(p)$, which have no physical meaning, appear in the lower troposphere (also around 350 mb) for all values of ϵ shown. They attain an appreciable size at 900 mb for $\epsilon=-0.4$. The

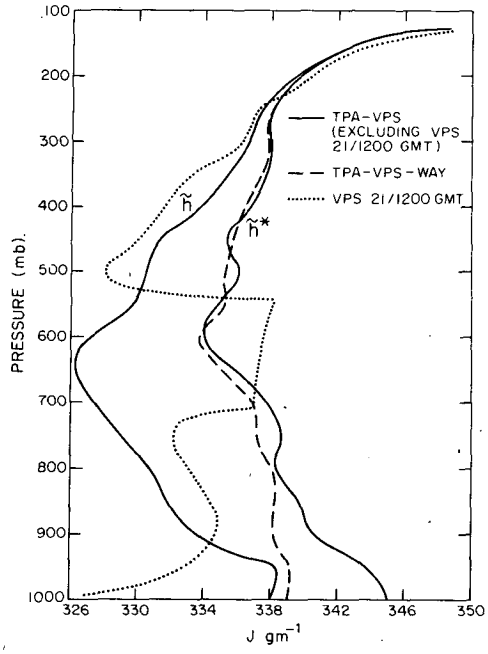

FIG. 14. Average moist static energies for northern Florida case study from 20/1200 GMT to 20/0000 GMT. Dotted line indicates anomalous VPS sounding that was excluded from the averages.

appearance of negative values of $m_B(p)$ is probably due to inaccuracies in the measured Q_1, Q_2 or Q_R, or may be caused by limitations in the cloud model itself.

We now attempt to determine an optimum value of ϵ by comparing model-computed and observed precipitation. In Fig. 17 condensation minus updraft evaporation $C-E_u$, precipitation at the ground P_g and downdraft E_d are shown as a function of ϵ for $\beta=0.75$

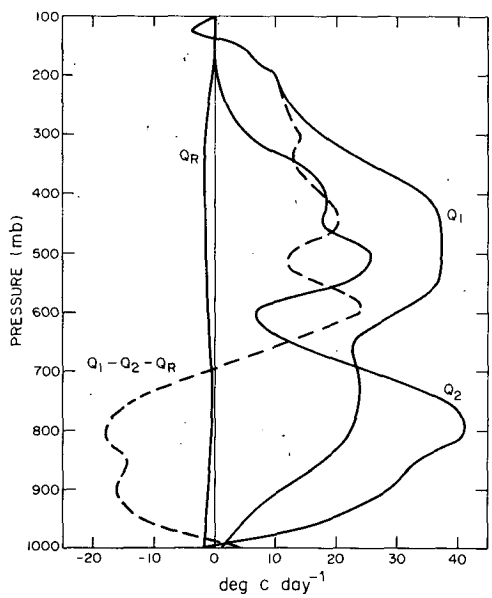

FIG. 15. Apparent heat source Q_1, apparent moisture sink Q_2 and radiative heating rate Q_R for northern Florida case study.

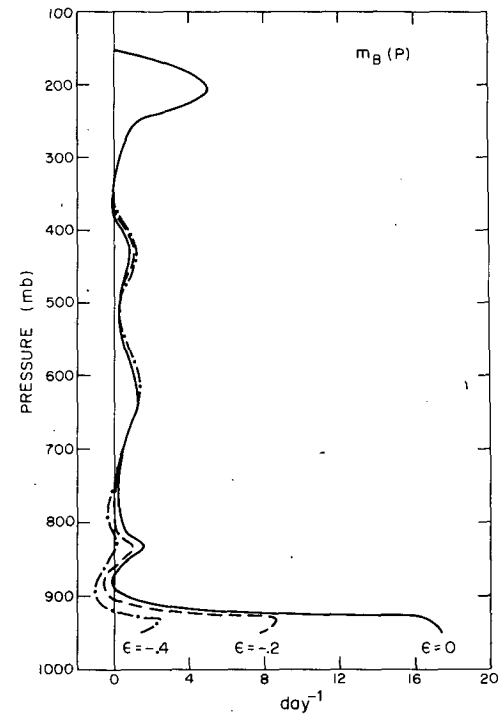

FIG. 16. Cloud-base mass flux distribution function $m_B(p)$ for northern Florida case study for three different downdraft intensities ($\epsilon=0$, -0.2, -0.4; $\beta=0.75$).

and $h_d(\lambda,p_0)=\tilde{h}^*(p_0)$. For this data set difficulty was encountered in obtaining positive values for E_u and for this reason we present the combination $C-E_u$. Recall that E_u is obtained by integrating $\bar{e}_u(p)$ through the depth of the cloud layer; however, $\bar{e}_u(p)$ is computed as a small residual in the water vapor continuity equation and is especially sensitive to errors in the

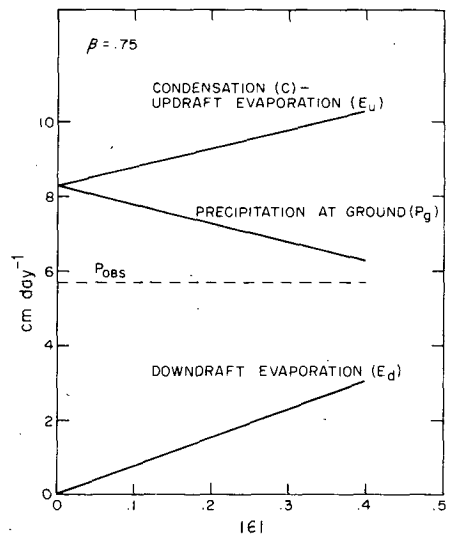

FIG. 17. Condensation minus updraft evaporation, precipitation at ground and downdraft evaporation as a function of ϵ for northern Florida case study ($\beta=0.75$).

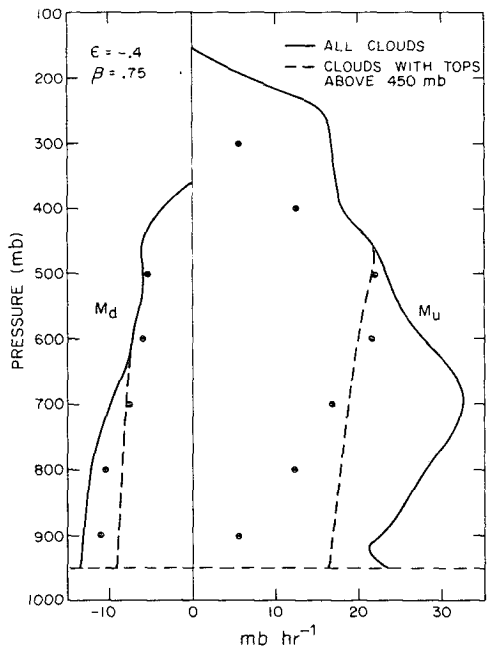

FIG. 18. Cumulus updraft and downdraft mass fluxes, M_u, M_d, from all clouds (solid lines) and clouds with tops above 450 mb (dashed lines) for $\epsilon=-0.4$, $\beta=0.75$. Large dots are Thunderstorm Project measurements taken from Table 2 of Braham (1952).

observational data. Precipitation at the ground P_g is 67% greater than the observed precipitation P_{OBS} for the no-downdraft case ($\epsilon=0$), but steadily decreases as $|\epsilon|$ increases, reaching a value within 10% of P_{OBS} at $\epsilon=-0.4$. Combining this result with the previous considerations, we select $\epsilon=-0.4$ as an optimum value for this data set. It is acknowledged that this conclusion is not entirely satisfactory considering the comparatively large negative values of $m_B(p)$ at $\epsilon=-0.4$.

The updraft and downdraft mass fluxes from all clouds and from deep cumulonimbi (those with tops above 450 mb) are shown in Fig. 18 for $\epsilon=-0.4$, $\beta=0.75$. Mass flux results are presented in this second form in order to make a meaningful comparison with Thunderstorm Project measurements, of which approximately half were made in Florida cumulonimbus clouds (near Orlando). Braham (1952) computed the average vertical mass fluxes within thunderstorm updrafts and downdrafts obtained by aircraft measurements of their widths and intensities. The average mass fluxes presented in his Table 2 are indicated in Fig. 18 by large dots, where the updraft peak magnitude in Braham's results have been normalized to the peak magnitude in M_u for the deep clouds. The general agreement in the shape of the updraft profile M_u with Thunderstorm Project measurements is felt to be quite good. The fact that the peak in M_u is at a slightly higher level than the Project measurements and is greater than the measured values in the upper troposphere may be, in part, due to the effect of Ohio thunderstorms (which are probably not as deep as Florida thunderstorms) being included in the average. This departure from the measured values (also in the lower troposphere) might further be related to the nature of the plume updraft model which, for clouds having tops where $m_B(p)$ is large ($\lambda<0.05$ km^{-1}), gives individual cloud-mass fluxes that increase only slowly with height.

An encouraging result seen in Fig. 18 is the agreement between the computed downdraft mass flux from deep cumulonimbi for $\epsilon=-0.4$, $\beta=0.75$ and the Thunderstorm Project measurements. The same normalization factor that was applied to the updraft measurements has been applied to those for the downdraft. Braham (1952) states that the relative magnitude of the updraft and downdraft mass fluxes that he computed are thought to be correct within 10% for summer thunderstorms in the eastern and southern United States.

The reduction in the net cumulus mass flux M_c and environmental sinking $\tilde{M}$ due to the effects of cumulus downdrafts is shown in Fig. 19. In the absence of downdrafts, strong sinking in the environment is diagnosed in the lower troposphere (below 600 mb). When downdrafts are included, this strong sinking is reduced and even changes sign below 750 mb. In the layer from 600 to 300 mb environmental rising motion is evident, presumably in response to large-scale dynamical processes.

We have computed for this northern Florida data

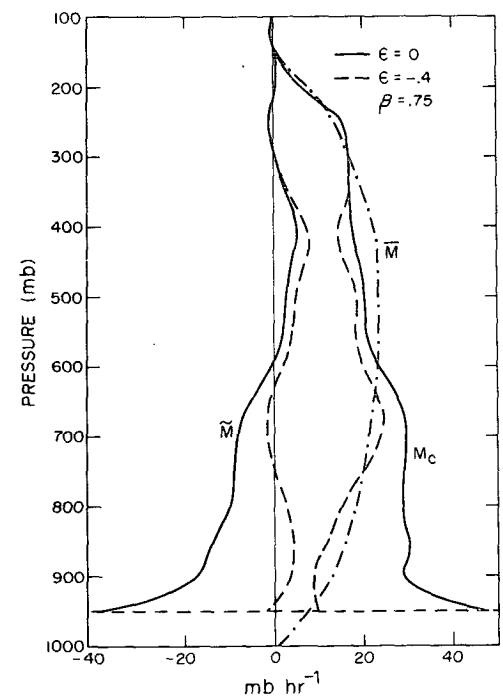

FIG. 19. Mean, environmental and cumulus mass fluxes with and without downdrafts for northern Florida case study ($\epsilon=0$, -0.4, $\beta=0.75$).

set the surface vertical eddy heat flux F_0 from

$$F_0=\frac{1}{g}\int_{p_T}^{p_s}(Q_1-Q_2-Q_R)dp,$$

where $F_0 \equiv S_0+LE_0$, S_0 is the sensible heat flux at the surface and E_0 the surface evaporation. For the period 20/1200 GMT to 22/0000 GMT we obtain $F_0=477$ W m^{-2} (985 cal cm^{-2} day^{-1}). If the Bowen ratio (S_0/LE_0) is small, as we might expect it to be for the rain-soaked ground in this region, then this result implies an exceedingly large evaporation rate, $\sim$1.5 cm day^{-1}. This discrepancy is difficult to explain. We note that for the Reed and Recker wave-trough region it was found that evaporation determined from Q_1, Q_2, Q_R exceeded that computed by the bulk aerodynamic method by a factor of 1.7 (see also Cho and Ogura, 1974). Similarly, Yanai *et al.* (1973) for their Marshall Islands data set found the evaporation computed from F_0 to be about twice that determined by the bulk aerodynamic method. Explanation for the systematic difference between the two independent estimates of evaporation is not apparent. We can only say that inaccuracies in the computed divergence (and, hence, vertical velocity) fields are probably introducing errors into Q_1 and Q_2 that are finally reflected in F_0. Although it is felt that the basic conclusions of this section with regard to the role of convective downdrafts are largely independent of this inconsistency in the observational data, further testing would appear to be necessary to support this claim.

5. Summary and concluding remarks

A diagnostic model has been developed to determine the effects of convective-scale updrafts and downdrafts on the thermodynamic properties of the large-scale atmospheric circulation. One-dimensional entraining plume models are used for both cumulus updrafts and downdrafts. A population of clouds having updrafts reaching to various heights in the troposphere, each with a unique rate of mass entrainment and each possessing a corresponding downdraft, is assumed to account for the total convective sensible and latent heat transports. An integral equation for a function representing the cloud-base mass flux for each type of cloud is derived using an assumption that relates the intensities of the updraft and downdraft.

The model has been tested in two different tropical (or near-tropical) regions: the western Pacific, using the Reed and Recker (1971) data set, and northern Florida, in the study of a tropical depression. It was found that convective-scale downdrafts are indeed important contributors to the total cumulus transport of mass, heat and water vapor in synoptic-scale convective disturbances. Mass fluxes in cumulus downdrafts in the Reed and Recker wave trough were determined to be approximately one-fourth the magnitude of those in cumulus updrafts in the lower troposphere. Houze and Leary (1976) have recently obtained convective mass transports for this data set that are substantially in agreement with these based on a method that uses quantitative radar measurements of cumulus clouds. In the western Pacific study, independent estimates of the relative intensities of updrafts and downdrafts (parameter ϵ) were made based on comparison of model-predicted precipitation with observed precipitation and on examination of the subcloud-layer moisture budget. Results from the northern Florida tropical depression case study indicate that cumulus downdraft mass fluxes are an even greater fraction (nearly one-half) of the updraft mass flux in the lower troposphere. The computed downdraft mass transports were found to be consistent with observations of thunderstorms over Ohio and Florida taken during the Thunderstorm Project (Byers and Braham, 1949).

Studies in both regions show that during convectively disturbed conditions shallow cumuli do not contribute as significantly to the total cloud-base mass flux as previously thought (Ogura and Cho, 1973; Cho and Ogura, 1974). We have shown that the neglect of cumulus-scale downdrafts accounts for the results obtained in these earlier studies. Measurements necessary to confirm this result are extremely difficult to obtain. Determination of mass fluxes in these small clouds using radar measurements in the manner proposed by Austin and Houze (1973) is not possible because of their negligible liquid water content. Measurements by Malkus (1954) of tradewind cumuli have shown these shallow clouds do not have organized downdrafts like those associated with cumulonimbi. It would appear that individual cloud measurements of this type combined with cloud census evaluations are necessary to determine the contribution by shallow cumuli to the total cumulus mass flux.

The results of this study also have implications on theories for the parameterization of cumulus convection, in particular, those of Ooyama (1971) and Arakawa and Schubert (1974). Details of the closure hypotheses that these authors have advanced will not be discussed here. In these theories cumulus clouds are assumed to contain only updrafts. The predictive equations for the large-scale temperature and water vapor fields no not, therefore, contain the downdraft terms $M_d\partial\bar{s}/\partial p$ and $M_d\partial\bar{q}/\partial p$ that appear in (23) and (22) of this paper; otherwise the equations are identical. Since these terms represent environmental lifting compensating cumulus downdraft mass flux, their neglect will lead to predictions of excessive warming and drying in the lower troposphere. The extent of this effect will depend on the nature of the closure assumptions employed. There is some evidence to indicate that the effects we have described are correct. Rosenthal (1973) has incorporated the parameterization theory of Ooyama into a two-dimensional, axisymmetric hurri-

cane model. Rosenthal finds that the Ooyama parameterization leads to a very realistic simulation of the hurricane structure in the upper troposphere. In the lower troposphere, however, unrealistic heating and drying are observed in the highly convective region extending outward from the 50 km radius of the storm. Excessive heating rates of $\sim 0.5°C\ day^{-1}$ and drying rates of $\sim 2.0\ g\ kg^{-1}\ day^{-1}$ were found to occur. It is felt that the neglect of downdrafts may account for these unrealistic features of the hurricane structure.

Although some success has been achieved with the diagnostic model, we must point out several important limitations. First, we note that since updraft detrainment is assumed to occur at a single level (cloud top), the effect of lateral detrainment over the life cycle of each cloud is not taken into account (Fraedrich, 1973; Betts, 1975). Detrainment from the cloud population within the context of the plume model can only be crudely represented by cloud-top detrainment from a continuous distribution of cloud sizes. The effect this deficiency of the plume model has on computed cloud population properties needs further investigation. Second, the downdraft model is a highly simplified one. Entrainment of air into the downdraft that has passed through an adjacent updraft is not considered. Both updrafts and downdrafts are assumed to entrain the same environmental air. The mechanism responsible for the formation of the downdraft is not explicitly taken into account. Rather, the magnitude of the downdraft mass flux (relative to that of the updraft) is specified through the parameter ϵ and the downdraft depth through the parameter β. In the determination of an optimum ϵ we have assumed that the air within downdrafts is at or near saturation. If this is not the case, an even greater mass flux within downdrafts will be diagnosed since the evaporation rate in unsaturated downdrafts is less.

A further consideration necessary in the development of cumulus parameterization theories is the large-scale transport of momentum by updrafts and downdrafts. Substantial downward transport of horizontal momentum may exist in connection with strong downdrafts from severe thunderstorms, squall lines, etc. Reed and Johnson (1974b) have shown that in the trough region of the Reed and Recker composite easterly wave, significant vertical transport of vorticity exists that is largely explainable in terms of dynamical processes associated with deep cumulonimbi. Further efforts are necessary to include the effects on momentum transport by clouds of all sizes.

Attempts at verification of the model put forth here would seem to rely most heavily on results of field experimentation. It is not yet clear whether the quality and resolvability of GATE data are sufficient to provide a more definitive determination of properties of cumulus downdrafts and their associated transports. In particular, it has been seen that accurate rainfall measurements are necessary to establish the relative intensities of updrafts and downdrafts deduced from synoptic-scale observations. Although selection of optimum values of β and ϵ has been made based on large-scale budget considerations, these quantities should ideally be determined from measurements of individual clouds ranging throughout the entire spectrum of cloud sizes. It is suggested that future field projects of this nature have as one important objective the detailed measurement of the properties of convective-scale downdrafts, their influence on the structure of the lower troposphere, and their modification of sensible and latent heat fluxes from the earth's surface.

Acknowledgments. I would like to thank Prof. Richard J. Reed for advice and encouragement during the course of this work. I also thank Prof. Robert A. Houze for his continual interest and helpful suggestions, Prof. James R. Holton for helpful discussions and Dr. Stanley L. Rosenthal and Hugh Willoughby for reading the manuscript. The assistance of Ernest Recker in data preparation and Robert Thompson for the analysis of precipitation data for the Florida case study has been appreciated. The research was supported by the National Science Foundation under Grant GA-32439.

APPENDIX

Water Vapor Budget Computation

Using the triangle of radiosonde stations VPS–WAY–TPA, horizontal divergences at each standard level of the soundings were computed using

$$\overline{\nabla\cdot\mathbf{v}}=\frac{1}{A}\oint v_n dl,$$

where A is the area of the triangle, dl a line element on the perimeter, v_n the component of the wind normal to the boundary, and the overbar denotes the area average. Vertical velocities were subsequently computed from

$$\omega(p)=\int_p^{p_s}(\overline{\nabla\cdot\mathbf{v}})_c\,dp,$$

where $(\overline{\nabla\cdot\mathbf{v}})_c$ is the corrected divergence given by

$$(\overline{\nabla\cdot\mathbf{v}})_c=\overline{\nabla\cdot\mathbf{v}}-\frac{1}{p_s-p_T}\int_{p_T}^{p_s}\overline{\nabla\cdot\mathbf{v}}dp,$$

p_s is the surface pressure and $P_T=70$ mb. Thus, vertical velocity vanishes at p_s and p_T when the divergences are mass-balanced in this manner.

Precipitation rates (P) were determined from

$$P-E_0=\frac{1}{g}\int_{p_s}^{p_T}\frac{\partial\tilde{q}}{\partial t}dp+\frac{1}{g}\int_{p_s}^{p_T}\overline{\mathbf{v}\cdot\nabla q}dp+\frac{1}{g}\int_{p_s}^{p_T}\tilde{q}(\overline{\nabla\cdot\mathbf{v}})_c dp,$$

where E_0 is the surface evaporation. Moisture storage was computed by taking the difference between $\tilde{q}$ 12 h before and after each central time. Horizontal advection of water vapor was determined by fitting a plane surface to q at the triangle vertices. The upper limit of integration p_T was necessarily changed to 300 mb, since relative humidity measurements were unavailable above this level; however, water vapor contents are so low above 300 mb that the contribution in this region to P is less than 1%.

REFERENCES

Arakawa, A., 1971: A parameterization of cumulus convection and its application to numerical simulation of the tropical general circulation. *Bull. Amer. Meteor. Soc.*, **52**, 783.

——, and W. Schubert, 1974: Interaction of a cumulus cloud ensemble with the large-scale environment, Part I. *J. Atmos. Sci.*, **31**, 674–701.

Austin, P. M., and R. A. Houze, 1973: A technique for computing vertical transports by precipitating cumuli. *J. Atmos. Sci.*, **30**, 1100–1111.

Betts, A. K., 1973a: A composite mesoscale cumulonimbus budget. *J. Atmos. Sci.*, **30**, 597–610.

——, 1973b: Nonprecipitating cumulus convection and its parameterization. *Quart. J. Roy. Meteor. Soc.*, **99**, 178–196.

——, 1974: The scientific basis and objectives of the U. S. Convection Subprogram for the GATE. *Bull. Amer. Meteor. Soc.*, **55**, 304–313.

——, 1975: Parametric interpretation of trade-wind cumulus budget studies. *J. Atmos. Sci.*, **32**, 1934–1945.

Braham, R. R., 1952: The water and energy budgets of the thunderstorm and their relation to thunderstorm development. *J. Meteor.*, **9**, 227–242.

Brown, J. M., 1974: Mesoscale motions induced by cumulus convection: A numerical study. Ph.D. thesis, Massachusetts Institute of Technology, 206 pp.

Byers, H. R., 1965: *Elements of Cloud Physics*. The University of Chicago Press, 191 pp.

——, and R. R. Braham, 1949: *The Thunderstorm*. Government Printing Office, Washington, D. C., 287 pp.

Cho, H. R., and Y. Ogura, 1974: A relationship between cloud activity and low-level convergence as observed in Reed-Recker's composite easterly waves. *J. Atmos. Sci.*, **31**, 2058–2065.

Delves, L. M., and J. Walsh, 1974: *Numerical Solution of Integral Equations*. Clarendon Press, 339 pp.

Dopplick, T. G., 1972: Radiative heating of the global atmosphere. *J. Atmos. Sci.*, **29**, 1278–1294.

Esbensen, S., 1975: An analysis of subcloud-layer heat and moisture budgets in western Atlantic trades. *J. Atmos. Sci.*, **32**, 1921–1933.

Fraedrich, K., 1973: On the parameterization of cumulus convection by lateral mixing and compensating subsidence. Part I. *J. Atmos. Sci.*, **30**, 408–413.

Frank, N. L., 1970: Atlantic tropical systems of 1969. *Mon. Wea. Rev.*, **98**, 307–314.

Garstang, M., 1967: Sensible and latent heat exchange in low-latitude synoptic scale systems. *Tellus*, **19**, 492–509.

Houze, R. A., and C. A. Leary, 1976: Comparison of convective mass and heat transports in tropical easterly waves computed by two methods. *J. Atmos. Sci.*, **33**, 424–429.

Johnson, R. H., 1975: The role of convective-scale precipitation downdrafts in cumulus and synoptic-scale interactions. Ph.D. dissertation, University of Washington, 136 pp.

Kamburova, P. L., and F. H. Ludlam, 1966: Rainfall evaporation in thunderstorm downdraughts. *Quart. J. Roy. Meteor. Soc.*, **92**, 510–518.

Malkus, J. S., 1954: Some results of a trade-cumulus investigation. *J. Meteor.*, **11**, 220–237.

——, 1955: On the formation and structure of downdrafts in cumulus clouds. *J. Meteor.*, **12**, 350–354.

——, 1960: Large-scale air-sea interactions. *The Sea*, Vol. 1, Wiley, 81–294.

Miller, M. J., and R. P. Pearce, 1974: A three-dimensional primitive equation model of cumulonimbus convection. *Quart. J. Roy. Meteor. Soc.*, **100**, 133–154.

Newton, C. W., 1966: Circulations in large sheared cumulonimbus. *Tellus*, **18**, 699–713.

Nitta, T., 1975: Observational determination of cloud mass flux distributions. *J. Atmos. Sci.*, **32**, 73–91.

——, and S. Esbensen, 1974: Heat and moisture budget analysis using BOMEX data. *Mon. Wea. Rev.*, **102**, 17–28.

Ogura, Y., and H. -R. Cho, 1973: Diagnostic determination of cumulus cloud populations from observed large-scale variables. *J. Atmos. Sci.*, **30**, 1276–1286.

——, and ——, 1974: On the interaction between the subcloud and cloud layers in tropical regions. *J. Atmos. Sci.*, **31**, 1850–1859.

Ooyama, K., 1971: A theory on parameterization of cumulus convection. *J. Meteor. Soc. Japan*, **49** (Special Issue), 744–756.

Reed, R. J., and E. E. Recker, 1971: Structure and properties of synoptic-scale wave disturbances in the equatorial western Pacific. *J. Atmos. Sci.*, **28**, 1117–1133.

——, and R. H. Johnson, 1974a: Diagnosis of cloud-population properties in tropical easterly waves. *Preprints Intern. Tropical Meteorology Meeting*, Nairobi, Kenya, Amer. Meteor. Soc., 50–56.

——, and ——, 1974b: The vorticity budget of synoptic-scale wave disturbances in the tropical western Pacific. *J. Atmos. Sci.*, **31**, 1784–1790.

Riehl, H., and J. S. Malkus, 1958: On the heat balance in the equatorial trough zone. *Geophysica*, **6**, 503–538.

——, and R. P. Pearce, 1968: Studies on interaction between synoptic and mesoscale weather elements in the tropics. Atmos. Sci. Pap. No. 126, Colorado State University, Ft. Collins. [Available from NTIS: No. PB 185718].

Rosenthal, S. L., 1973: Hurricane modeling experiments with a new parameterization for cumulus convection. NOAA Tech. Memo. ERL WMPO-4, 41 pp. [Available from NTIS: No. COM 7311530].

Sanders, F., and R. J. Paine, 1975: The structure and thermodynamics of an intense mesoscale convective storm in Oklahoma. *J. Atmos. Sci.*, **32**, 1563–1579.

Squires, P., and J. S. Turner, 1962: An entrainment jet model for cumulonimbus updrafts. *Tellus*, **14**, 422–434.

Wilhelmson, R., 1974: The life cycle of a thunderstorm in three-dimensions. *J. Atmos. Sci.*, **31**, 1629–1651.

Yanai, M., 1971: The mass, heat and moisture budgets and the convective heating within tropical cloud clusters. *Bull. Amer. Meteor. Soc.*, **52**, 767.

——, S. Esbensen and J. -H. Chu, 1973: Determination of bulk properties of tropical cloud clusters from large-scale heat and moisture budgets. *J. Atmos. Sci.*, **30**, 611–627.

Zipser, E. J., 1969: The role of organized unsaturated convective downdrafts in the structure and rapid decay of an equatorial disturbance. *J. Appl. Meteor.*, **8**, 799–814.

——, 1970: The Line Islands Experiment, its place in tropical meteorology and the rise of the fourth school of thought. *Bull. Amer. Meteor. Soc.*, **51**, 1136–1146.